Impacts of ice-shelf melting on water mass transformation in the Southern Ocean from E3SM simulations

Hyein Jeong*, Xylar S. Asay-Davis, Adrian K. Turner, Darin S. Comeau, Stephen F. Price

Los Alamos National Laboratory, Los Alamos, NM 87545, USA

Ryan P. Abernathey

Lamont-Doherty Earth Observatory of Columbia University, Palisades, NY 10964, USA

Milena Veneziani, Mark R. Petersen, Matthew J. Hoffman

Los Alamos National Laboratory, Los Alamos, NM 87545, USA

Matthew R. Mazloff

Scripps Institution of Oceanography, La Jolla, CA 92093, USA

Todd D. Ringler

Los Alamos National Laboratory, Los Alamos, NM 87545, USA

**Corresponding author address:* Hyein Jeong, Theoretical Division, Los Alamos National Laboratory, PO Box 1663, Los Alamos, NM 87545.

E-mail: hijeong@lanl.gov, hijeong820310@gmail.com

Early Online Release: This preliminary version has been accepted for publication in *Journal of Climate*, may be fully cited, and has been assigned DOI 10.1175/JCLI-D-19-0683.1. The final typeset copyedited article will replace the EOR at the above DOI when it is published.

ABSTRACT

Accepted for publication in *Journal of Climate*. DOI 10.1175/JCLI-D-19-0683.1.

The Southern Ocean overturning circulation is driven by winds, heat fluxes, and freshwater sources. Among these sources of freshwater, Antarctic sea-ice formation and melting play the dominant role. Even though ice-shelf melt is relatively small in magnitude, it is located close to regions of convection, where it may influence dense water formation. Here, we explore the impacts of ice-shelf melting on Southern Ocean water mass transformation (WMT) using simulations from the Energy Exascale Earth System Model (E3SM) both with and without the explicit representation of melt fluxes from beneath Antarctic ice shelves. We find that ice-shelf melting enhances transformation of Upper Circumpolar Deep Water (UCDW), converting it to lower density values. While the overall differences in Southern Ocean WMT between the two simulations are moderate, freshwater fluxes produced by ice-shelf melting have a further, indirect impact on the Southern Ocean overturning circulation through their interaction with sea-ice formation and melting, which also cause considerable upwelling. We further find that surface freshening and cooling by ice-shelf melting causes increased Antarctic sea-ice production and stronger density stratification near the Antarctic coast. In addition, ice-shelf melting causes decreasing air temperature, which may be directly related to sea-ice expansion. The increased stratification reduces vertical heat transport from the deeper ocean. Although the addition of ice-shelf melting processes leads to no significant changes in Southern Ocean WMT, the simulations and analysis conducted here point to a relationship between increased Antarctic ice-shelf melting and the increased role of sea ice in Southern Ocean overturning.

Accepted for publication in *Journal of Climate*. DOI 10.1175/JCLI-D-19-0683.1.

1. Introduction

The Southern Ocean plays a large role in Earth's climate system (Morrison et al. 2011; Marshall and Speer 2012; Séférian et al. 2012; Heuzé et al. 2013; Merino et al. 2018) as a significant sink for atmospheric heat (Roemmich et al. 2015) and anthropogenic carbon dioxide (Sallée et al. 2012), hence reducing global warming (Merino et al. 2018). The Southern Ocean also produces the densest water mass in the global ocean, Antarctic Bottom Water (AABW), which plays an active role in driving the global meridional overturning circulation (MOC). In turn, the freezing and melting of Antarctic sea ice are a major control on this overturning circulation. Using a water mass transformation (WMT) analysis (Walin 1982), Abernathey et al. (2016) revealed that differential brine rejection and sea-ice melting are strong controls on the strength of the MOC by governing the upwelling and transformation of Circumpolar Deep Water (CDW), with precipitation playing a more minor part.

Despite a recent sharply decreasing trend from 2014 to 2019 (Parkinson 2019), most observational studies report increasing Antarctic sea-ice extent during the last 40 years. Most CMIP5 models, however, simulate a steadily decreasing Antarctic sea-ice extent over the past few decades (Flato et al. 2013), failing to capture the observed expansion. Significant effort has gone into understanding the cause for this discrepancy, primarily through the investigation of changes in atmospheric climate modes and their relation to tropical forcing (Thompson et al. 2011; Turner et al. 2009; Stammerjohn et al. 2008; Li et al. 2014; Kwok et al. 2016), ozone depletion (Bitz and Polvani 2012; Sigmond and Fyfe 2010), and ocean and sea-ice feedbacks (Zhang 2007). Increased Antarctic ice-shelf melting could also be contributing to Antarctic sea-ice expansion through the freshening of Southern Ocean surface waters (Jacobs et al. 2002; Jacobs and Giulivi 2010; Bintanja et al. 2013; Merino et al. 2018). However ice sheet freshwater fluxes are typically not treated

Accepted for publication in *Journal of Climate*. DOI 10.1175/JCLI-D-19-0683.1.

realistically in CMIP climate models; freshwater enters the ocean at the ice sheet edge, is distributed near the sea surface, and temporal variability enters only through changes in precipitation. These simplifications may partially explain the failure of existing climate models to reproduce the observed Antarctic sea-ice trends (Turner et al. 2013; Zhang et al. 2019).

Ice-shelf melt fluxes, though relatively small in magnitude compared to freshwater fluxes from sea-ice freezing and melting or precipitation, may have a disproportionate influence on dense water formation because they occur at depth, forming a buoyant plume that contributes to ocean overturning. In addition to its direct impacts, ice-shelf melting contributes to freshwater fluxes indirectly through its impacts on stratification and circulation, which feeds back on sea-ice formation and melting (Hellmer 2004; Donat-Magnin et al. 2017; Jourdain et al. 2017; Mathiot et al. 2017). While not previously applied to simulations that include thermodynamic interactions with ice shelves, the WMT framework (Walin 1982; Abernathey et al. 2016) is an ideal tool for obtaining a more qualitative and quantitative understanding of how Antarctic ice-shelf melt fluxes impact Southern Ocean properties and circulation.

In this study, we investigate the impacts of Antarctic ice-shelf melting on Southern Ocean WMT and its indirect impacts on sea-ice formation and melting. Our approach is that of a sensitivity study, where a perturbed simulation includes an additional source of freshwater derived from explicitly calculating ice-shelf melt fluxes that is not present in the control. Although the amount of freshwater added to the perturbed simulation is about an order of magnitude larger than observed trends ($\sim$1400 Gt yr^{-1} $\approx$ 0.046 Sv, in our simulation vs. $\sim$155 Gt yr^{-1} $\approx$ 0.0049 Sv from observations; Bamber et al. 2018), this approach may suggest mechanisms by which increased ice-shelf melting, observed in Antarctica during the last few decades (e.g., Shepherd et al. 2004; Khazendar et al. 2016; Pritchard et al. 2012; Holland et al. 2019), could impact the broader climate. In Section 2, we briefly describe the E3SM climate model, the reference data sets used for model

Accepted for publication in *Journal of Climate*. DOI 10.1175/JCLI-D-19-0683.1.

validation, and the WMT analysis used herein. Section 3 analyzes the fidelity of E3SM's Southern Ocean climate compared to available reanalysis data sets. Section 4 uses the WMT framework to examine interactions between ice-shelf melting and Southern Ocean sea ice processes, and Section 5 provides a detailed analysis of the WMT caused by Antarctic ice-shelf melting. In Section 6, we present our summary and conclusions from this study.

2. Data and Methodology

a. E3SM

For this study we use the Energy Exascale Earth System Model (E3SM) version 1, a new global, coupled Earth system model developed by the U.S. Department of Energy (DOE) (Golaz et al. 2019; Petersen et al. 2019; Rasch et al. 2019). E3SM v1[1] features fully coupled ocean, sea-ice, river, atmosphere and land components as well as a unique capability for multi-resolution modeling using unstructured grids in all of its components. The ocean and sea-ice components of E3SM v1 are MPAS-Ocean and MPAS-Seaice respectively, which are built on the Model for Prediction Across Scale (MPAS) modeling framework (Ringler et al. 2013; Petersen et al. 2019) and share the same unstructured horizontal mesh. The ocean model vertical grid is a structured, z-star coordinate (Petersen et al. 2015; Reckinger et al. 2015) and uses 60 layers ranging in thickness from 10 m at the surface to 250 m in the deep ocean. The ocean and sea-ice mesh used here contain $\sim$230,000 horizontal ocean cells with resolution varying from 30 to 60 km; enhanced resolution in the equatorial and polar regions is used to better resolve processes of interest. Within the area of interest in this study (south of 60°S) the ocean and sea-ice horizontal resolution varies from 35 to 50km. Petersen et al. (2019) provide a more detailed description of the E3SM v1 ocean and sea-ice components. The atmosphere component of E3SM v1 is the E3SM Atmospheric Model

[1] https://github.com/E3SM-Project/E3SM/

Accepted for publication in *Journal of Climate*. DOI 10.1175/JCLI-D-19-0683.1.

(EAM), which uses a spectral element dynamical core at $\sim$100 km horizontal resolution on a cubed-sphere geometry. EAM's vertical grid is a hybrid, sigma-pressure coordinate and uses 72 layers with a top of atmosphere at approximately 60 km. Golaz et al. (2019), Xie et al. (2018), and Qian et al. (2018) provide a detailed description of the E3SM v1 atmosphere component. Since there is currently no coupled land ice component, E3SM v1 routes precipitation (snow or rain) that falls on Antarctica back to the rest of the climate system as either solid ice or liquid runoff, respectively. Snow in excess of 1 m water equivalent (so-called "snowcapping") and rain are immediately routed to the nearest coastal ocean grid cell and deposited at the surface with a small amount of horizontal smoothing. This functions as a crude approximation to unresolved ice sheet processes (including surface processes, iceberg calving, and basal melting) in order to keep the ice sheet in instantaneous equilibrium with climate forcing, and conserves mass globally to avoid having to account for a potentially large water sink in the model.

A new capability for Earth system models, now available in E3SM, is the extension of the ocean domain to include ocean circulation in cavities under Antarctic ice shelves. In these cavities, MPAS-Ocean solves the full prognostic equations, which include velocity, temperature, and salinity. Based on these fields, diagnostic melt fluxes at the base of the ice shelves are computed using coupled boundary conditions for heat and salt conservation, and a linearized equation of state for the freezing point of seawater (Holland and Jenkins 1999; Hellmer and Olbers 1989). These boundary conditions are used to simultaneously compute the potential temperature, salinity, and melt rate at the ice shelf base using a velocity-dependent parameterization of the transfer of heat and salt across the ocean-ice-shelf boundary layer (Dansereau et al. 2014) with constant, non-dimensional heat- and salt-transfer coefficients (Jenkins et al. 2010). The boundary conditions account only for the conversion of sensible heat from the ocean into latent heat of melting ice, ignoring the sensible heat flux into the ice (which is typically $\lesssim 10\%$ of other terms; Holland

Accepted for publication in *Journal of Climate*. DOI 10.1175/JCLI-D-19-0683.1.

and Jenkins 1999). The thermal and haline driving terms are computed using "far-field" potential temperature and salinity averaged over the top 10 m of the water column. The freshwater and heat fluxes from ice-shelf melting are deposited into the ocean at depth using an exponentially decaying distribution over the water column with a characteristic distance from the interface of 10 m. In the simulations presented here, melt fluxes are computed directly in the ocean component once during each ocean time step, rather than in the coupler. No overflow parameterizations, common in many ESMs of similar resolution (Briegleb et al. 2010), are used to redistribute water masses between ice-shelf cavities and the continental shelf or between the continental shelf and the deep ocean. Given that E3SM does not yet have the ice sheet-ocean coupling needed to model the response of the ice sheet to basal melting, we use a static geometry for the ice-shelf cavities and grounding line. Thus, we are able to model the impact of ice-shelf melt fluxes on ocean circulation and stratification, but not the feedback from ocean circulation and ice shelf basal melting on ice-sheet stability. Here, we assume that the term "ice-shelf melting" includes both melting and freezing (i.e., negative melting) at the base of the ice shelf, but we label it "melting" because that term is dominant.

To better understand and quantify the impact of these additional heat and freshwater fluxes in an Earth system model, we have run a pair of fully coupled, pre-industrial (Eyring et al. 2016) simulations with E3SM: one with ice-shelf melt fluxes (hereafter, "ISM")[2], and one without (hereafter, "Ctrl")[3]. Previously published E3SM simulations (Golaz et al. 2019; Petersen et al. 2019) do not include ice-shelf cavities, but the horizontal and vertical grids are otherwise identical to these. Both ISM and Ctrl include the three-dimensional ocean domain below the ice shelves, but in Ctrl the ice-shelf base is simply a depressed surface where no heat and freshwater exchange occur.

[2]Full name in E3SM archive: 20180612.B_case.T62_oEC60to30v3wLI.modified_runoff_mapping.edison

[3]Full name in E3SM archive: 20180612.B_case.T62_oEC60to30v3wLI.modified_runoff_mapping.no_melt_fluxes.edison

Accepted for publication in *Journal of Climate*. DOI 10.1175/JCLI-D-19-0683.1.

This experimental setup can be thought of as a sophisticated freshwater hosing experiment, where the amount, timing, and location of the additional freshwater input to the system is model-state dependent. While both simulations have runoff from Antarctic precipitation, the ISM simulation has an additional source term of freshwater through ice-shelf basal melting ($\approx$0.045 Sv) that is not in the Ctrl simulation (see Table 1 and Fig. 1). This difference in the freshwater budget has the effect of an additional heat sink in the ISM simulation, since the freshwater from ice-shelf melting is deposited in the ocean at the pressure- and salinity-dependent freezing point. The simulations use "cold-start" initial conditions; the ocean is initialized with a month-long spin-up (without ice-shelf melting) from rest for initial adjustment, and sea ice is initialized with a 1 meter-thick disk of ice extending to 65° in both hemispheres. Each simulation was run for 75 years, with model data from the last 30 years used for analysis.

b. Atmosphere, ocean and sea-ice state estimates

Before investigating the impacts of ice-shelf melting on WMT, we assess E3SM's simulated ocean temperature, salinity, and sea-ice properties over the Southern Ocean. To do this, we compare E3SM results to several data sets including direct observations, model-based state estimates, and interpolated climatologies of the ocean and sea-ice in this region. The Southern Ocean State Estimate (SOSE, Mazloff et al. 2010) is a state-of-the-art data-assimilation product that incorporates millions of ocean and sea-ice observations while maintaining dynamically consistent ocean state variables. Given the sparsity of observations in many regions around Antarctica, SOSE offers a comprehensive, physically based estimate of ocean properties that would otherwise be entirely uncharacterized. We also use the U.K. Met Office's observational data sets (EN4; Good et al. 2013), the World Ocean Atlas 2018 (WOA18; Locarnini et al. 2018), and the World Ocean Circulation Experiment (WOCE)/Argo Global Hydrographic Climatology (WAGHC; Gouretski

Accepted for publication in *Journal of Climate*. DOI 10.1175/JCLI-D-19-0683.1.

2018), each of which provides a global data product of the subsurface ocean temperature and salinity. For comparison of atmospheric winds over the Southern Ocean, we use zonal wind stress from NCEP/NCAR Reanalysis I (Kalnay et al. 1996). For the sea-ice evaluation, we use several satellite-derived observational data sets: sea-ice concentration from the SSM/I NASA Team (Cavalieri et al. 1996) and SSM/I Bootstrap (Comiso 1999) and sea-ice thickness from ICESat (Kurtz and Markus 2012).

We note that these ocean and sea-ice data sets represent present-day conditions, whereas the E3SM simulations are representative of model conditions for the the pre-industrial climate. While there will be uncertainty when comparing pre-industrial simulation output with present-day observations, we find that the differences between pre-industrial and present-day control simulations are much less than the differences between different model configurations under the same pre-industrial forcing. Therefore, as in other studies (e.g., Menary et al. 2018), we feel justified in using present-day observations as a metric by which to judge our pre-industrial simulation output. Detailed information about each of these data sets, which have been time-averaged as indicated, is provided in Table 2.

c. Surface-flux driven water mass transformation

Water mass transformation analysis, first introduced by Walin (1982), quantifies the relationship between the thermodynamic transformation of water mass properties within an ocean basin and the net transport of those same properties into or out of the basin. This relationship has been used to infer Southern Ocean overturning circulation based on observations of air-sea fluxes and to characterize the thermodynamic processes that sustain the Southern Ocean overturning in models (Abernathey et al. 2016). Here, we apply a WMT analysis framework (following Abernathey et al. 2016) to aid in our investigation of Southern Ocean interactions between the atmosphere,

Accepted for publication in *Journal of Climate*. DOI 10.1175/JCLI-D-19-0683.1.

ocean, sea ice, and ice shelves, and to help identify biases in the E3SM's representation of these processes.

Southern Ocean water masses are assumed to be primarily transformed by surface heat and freshwater fluxes (Abernathey et al. 2016). As sea-ice grows, brine rejection (the result of a surface flux of freshwater out of the ocean) and vertical mixing have a tightly coupled relationship and contribute along with other surface fluxes to transformations (Abernathey et al. 2016). In addition, geothermal heating or internal tide and lee wave-driven mixing can also contribute to WMT in Southern Ocean, affecting formation or consumption of AABW (De Lavergne et al. 2016). Furthermore, Groeskamp et al. (2016) showed that cabbeling and thermobaricity also play a significant role in the WMT budget, with cabbeling having a particularly important role in the formation of Antarctic Intermediate Water (AAIW) and AABW. Mixing-induced, interior diabatic fluxes, however, are not explicitly diagnosed in our simulations. Consequently, we only consider the transformation rate induced by surface fluxes.

The transformation across density surfaces is diagnosed from surface heat and freshwater buoyancy fluxes:

$$\Omega(\sigma_k,t) = -\frac{1}{\sigma_{k+1}-\sigma_k}\iint_A\left(\frac{\alpha Q_{net}}{\rho_0 C_p}\right)dA + \frac{1}{\sigma_{k+1}-\sigma_k}\iint_A\left(\frac{\beta SF_{net}}{\rho_0}\right)dA, \tag{1}$$

where variables in Equation 1 are defined in Table 3. In this study, the total WMT into the ocean consists of the transformation rate due to net surface heat flux (the first term of right-hand side in Equation 1) and the transformation rate due to net surface freshwater flux (the second term of right-hand side in Equation 1). The WMT is calculated numerically by discretizing potential density, σ_k, into 400 unevenly spaced bins. The bin spacing, $\sigma_{k+1}-\sigma_k$, varies from 0.025 $\mathrm{kg\,m^{-3}}$ at low densities to 0.0025 $\mathrm{kg\,m^{-3}}$ at high densities. This density spacing was chosen by Abernathey et al.

Accepted for publication in *Journal of Climate*. DOI 10.1175/JCLI-D-19-0683.1.

(2016) who showed that it provides good resolution for high-density, polar water masses. In this study, we analyze the WMT rate south of 60°S.

All sources of net surface heat and freshwater fluxes are communicated to the ocean component through the coupler from the respective model components (e.g. precipitation from the atmosphere component). The exception to this are the ice-shelf melt fluxes, which, in the absence of a dynamic land-ice component, are calculated directly in the ocean component. Each term is stored separately in ocean history files. Here, "surface" implies processes at the atmosphere/ocean interface, but also at the sea ice/ocean and ice shelf/ocean interfaces. That is, the surface considered here is always the ocean surface regardless of what other model component that surface is in contact with.

To diagnose the role of different surface freshwater fluxes, we decompose surface net freshwater flux, F_{net}, into several sources:

$$F_{net} = F_{A\to O} + F_{I\to O} + F_{S\to O}, \tag{2}$$

where, $F_{A\to O}$ is the freshwater flux from the atmosphere into the ocean, $F_{I\to O}$ is that from sea-ice into the ocean and $F_{S\to O}$ is that from ice shelves into the ocean. $F_{I\to O}$ is further decomposed into two parts: the freshwater flux from sea-ice formation ($F_{\text{formation}}$) and that from sea-ice melting (F_{melting}):

$$F_{\text{formation}} = F_{I\to O} \text{ where } F_{I\to O} < 0, \tag{3}$$

$$F_{\text{melting}} = F_{I\to O} \text{ where } F_{I\to O} > 0. \tag{4}$$

The water mass formation (WMF) rate is the difference of the transformation rate with respect to density surfaces,

$$M(\sigma) = -[\overline{\Omega(\sigma_{k+1})} - \overline{\Omega(\sigma_k)}], \tag{5}$$

where the over-bar represents an average in time.

Accepted for publication in *Journal of Climate*. DOI 10.1175/JCLI-D-19-0683.1.

The transformation and formation rate are computed with respect to surface-referenced potential density, but plotted against the neutral density, γ_n, using a regression relationship between potential density and neutral density (Jackett and McDougall 1997; Klocker et al. 2009). This is possible because surface-referenced potential density and neutral density have a robust linear relationship in the upper ocean (Abernathey et al. 2016). Table 4 shows how the WMT and formation rates should be physically interpreted with respect to their sign.

Since we focus on the region south of 60°S, we classify Southern Ocean water masses into Surface Water ($\gamma_n < 27.5\ \mathrm{kg\,m^{-3}}$), Upper Circumpolar Deep Water (UCDW; $27.5 < \gamma_n < 28.0\ \mathrm{kg\,m^{-3}}$), Lower Circumpolar Deep Water (LCDW; $28.0 < \gamma_n < 28.2\ \mathrm{kg\,m^{-3}}$), and Antarctic Bottom Water (AABW; $\gamma_n > 28.2\ \mathrm{kg\,m^{-3}}$).

3. Southern Ocean climate in E3SM

Before looking in more detail at the impacts of ice-shelf melting on WMT in E3SM, we investigate the fidelity of ocean temperature and salinity in simulation results from E3SM. In this section, we use the Ctrl simulation to investigate the simulated Southern Ocean climate. Here, we make comparisons to the Ctrl simulation rather than the ISM simulation for three main reasons. First, the Ctrl configuration is closer to the "standard" E3SM configuration that has been used to run the CMIP6 DECK experiments (Golaz et al. 2019). Second, while the ISM configuration might be considered to represent freshwater fluxes in a more physically realistic way, the state of its climate has received less assessment and scrutiny to date. Finally, Ctrl is also the configuration more similar to other ESMs used for CMIP experiments.

Temperature and salinity are the most important characteristics of seawater, in that they control ocean density and govern the vertical movement of ocean water. Fig. 2a through d show E3SM's annual mean climatology for temperature and salinity at the sea-surface and at 500 m depth over

Accepted for publication in *Journal of Climate*. DOI 10.1175/JCLI-D-19-0683.1.

the Southern Ocean (south of 50°S). The Southern Ocean is the coldest part of the global ocean, and is also relatively fresh, with an area-averaged sea-surface temperature (SST) of 1.50°C and sea-surface salinity (SSS) of 33.6 PSU in E3SM (Fig. 2a and b). At 500 m depth the temperature and salinity is relatively warm and salty compared to the sea-surface, with an area-averaged temperature of 2.43°C and salinity of 34.5 PSU (Fig. 2c and d). These relatively high temperatures can lead to ice shelf melting. In Fig. 2e we compare E3SM's temperature and salinity with the four ocean products described in Section 2, in terms of area-weighted root mean square error (RMSE) at the sea-surface and 500 m depth. The scatter diagram shows that the RMSE of temperature and salinity at the sea-surface is larger than that at a depth of 500 m, indicating ~ 0.9°C and ~ 0.35 PSU errors at the sea-surface, and ~ 0.8°C and ~ 0.13 PSU errors at a depth of 500 m.

To investigate the characteristics of the potential temperature and salinity in the ocean interior, Fig. 3 shows the full-depth, volumetric T-S diagram of the Southern Ocean for E3SM and the four ocean data products. The volumetric T-S diagram, first introduced by Montgomery (1958), presents a census for how much of a water mass has a given set of T-S properties (Thomson and Emery 2014). The Southern Ocean near Antarctica has the densest, coldest water in the global ocean. This dense water is referred to as AABW and is located at the bottom of the T-S diagram ($\gamma_n > 28.2$ kg m^{-3} in Fig. 3). In general, E3SM has AABW at a similar density to the four ocean data products, which may be attributable to the initial conditions given the relatively short model spin-up. There are some discrepancies, however, in the CDW and lighter water mass ranges ($\gamma_n < 28.2$ kg m^{-3}). In the CDW range E3SM has relatively warmer temperatures and lower salinities compared to the four ocean products.

It is also important to characterize how well E3SM represents that total water transported by ocean currents. In Fig. 4 we show the horizontal and overturning volume transport in the Southern Ocean for E3SM and SOSE. Positive values of the streamfunction in Fig. 4a, d show anticyclonic

Accepted for publication in *Journal of Climate*. DOI 10.1175/JCLI-D-19-0683.1.

subtropical gyres, while negative values represent cyclonic subpolar gyres. There is strong eastward transport by the Antarctic Circumpolar Current (ACC) between the subtropical and subpolar gyres, as shown by the rapidly increasing contours from approximately 0 to 170Sv in Fig. 4d. The results from SOSE suggest that the Weddell gyre transport is almost double that of the Ross Sea gyre. In general, E3SM simulates the horizontal volume transport well, as indicated by a reasonably high pattern correlation coefficient of 0.98 between the horizontal circulation patterns from SOSE and E3SM (Fig. 4a compared with d). The canonical value of net transport through Drake passage, the narrowest choke point of the ACC, is 134 $\pm$ 11.2 Sv from observational estimate (Whitworth and Peterson 1985; Cunningham et al. 2003), while recently Donohue et al. (2016) suggested the transport of 173.3 $\pm$ 10.7 Sv from updated observed data. E3SM simulates transport through the Drake Passage of 127 $\pm$ 11 Sv, which is a value that falls within the canonical observed range but is significantly lower than the more recent estimate.

The Meridional Overturning Circulation (MOC), calculated in depth space, does not reflect cross-isopycnal flow (Speer et al. 2000). However, it does clearly show the dominant Southern Ocean Ekman transport in E3SM and SOSE, which is due primarily to the strong atmospheric westerly winds around 50°S (Fig. 4b and e). Closer to Antarctica, Ekman divergence drives upwelling of deep waters (Fig. 4e). E3SM simulates the Southern Ocean overturning circulation reasonably well but displays Ekman transport that is stronger ($\sim$41 Sv) compared to SOSE ($\sim$33 Sv) and shifted equatorward (Fig. 4b), both of which are likely due to stronger westerly winds in E3SM around 50°S (Fig. 4c). Biases in westerly winds are common phenomena in CMIP5 simulations. Bracegirdle et al. (2013) found that every CMIP5 model shows an equatorward bias ranging from 0.4° to 7.7° in latitude. Also, there is a large spread in climatological zonal wind strength in the models compared to reanalysis data.

Accepted for publication in *Journal of Climate*. DOI 10.1175/JCLI-D-19-0683.1.

Since buoyancy fluxes from sea-ice formation and melting are the next most dominant terms, after westerly winds, in causing CDW to upwell (Abernathey et al. 2016) it is important to validate the properties of sea-ice in E3SM. Fig. 5 compares E3SM's June-July-August (JJA) and December-January-February (DJF) mean sea-ice concentration, October-November (ON) and February-March (FM) mean sea-ice thickness, and JJA and DJF mean freshwater flux from sea-ice into the Southern Ocean with satellite-based observations and SOSE. While E3SM simulates the summer sea-ice concentrations well (Fig. 5g and j), close to Antarctica, Southern Hemisphere winter sea-ice concentrations are higher than observations during the JJA season (Fig. 5a and d). First, it is important to keep in mind that these simulations are based on pre-industrial conditions, and this may mean that sea-ice concentration should not be expected to match present-day observations. Second, this kind of bias is common in CMIP5 models, which while simulating the seasonal cycle of sea-ice concentration well, show large variability from model to model in sea-ice extent (Flato et al. 2013). There are a number of ways in which sea ice is influenced by and interacts with the atmosphere and ocean, and some of these feedbacks are still poorly quantified (Flato et al. 2013). E3SM has relatively thicker sea ice compared to ICESat (Ice, Cloud, and land Elevation Satellite) during October-November and February-March (Fig. 5 middle column). This is a point that should be revisited in the future, when improved sea-ice thickness observations from ICESat-2 become available in the Southern Ocean. E3SM and SOSE are similar with respect to patterns of JJA and DJF mean freshwater flux from sea-ice to ocean (Fig. 5 right column), but E3SM shows increased sea-ice formation (corresponding to a negative freshwater flux) near Antarctica during JJA and increased sea-ice melting (corresponding to a positive freshwater flux) offshore during the DJF season compared to SOSE.

Accepted for publication in *Journal of Climate*. DOI 10.1175/JCLI-D-19-0683.1.

The above discussion argues that E3SM does a reasonable job of capturing the salient features of Southern Ocean water masses, horizontal and overturning circulation, and sea-ice formation and melting. We now move on to a comparative analysis of the Ctrl and ISM simulations.

4. General impacts of ice shelf melting on hydrography, atmosphere, and sea-ice over the Southern Ocean

a. Impacts on the Southern Ocean

To investigate changes in hydrography over the Southern Ocean due to ice-shelf melting we show zonally averaged differences between the Ctrl and ISM simulations for ocean temperature, salinity, and potential density, for the specific basins of interest (the Amery ice-shelf sector, and the Ross, Amundsen, and Weddell Seas; Fig. 6). The first thing to note is that, in both the Ctrl and ISM simulations, isopycnals are weakly domed as they approach the continental shelf, especially in the Amery, Ross Sea and Weddell Sea sectors (Fig. 6b, e, k), indicating the presence of a weak Antarctic Slope Front. Furthermore, the ISM simulation has relatively fresher surface waters near Antarctica, as well as fresher subsurface waters inside the ice-shelf cavities (Fig. 6 left column). These salinity differences directly influence the potential density distribution; the ISM simulation shows lower densities relative to the Ctrl simulation at the surface as we approach Antarctica and in the subsurface over the shelf (Fig. 6 middle column). This behavior in the Amery Ice Shelf sector and Amundsen Sea, allows for the transport of relatively warm, deep water toward Antarctic ice-shelf cavities rather than ventilation of this water at the ocean surface farther offshore (dashed line in Fig. 6b, which continues to the ice shelves rather than impinging on the surface). The onshore transport of warm deep water results in more ice-shelf melting in the Amery and Amundsen Sea sectors in E3SM (Fig. 1a). For the Ross and Weddell Seas, the ISM simulation isopycnals im-

Accepted for publication in *Journal of Climate*. DOI 10.1175/JCLI-D-19-0683.1.

pinge more on the topography at depth, thus producing a relatively stronger Antarctic Slope Front and inhibiting transport of CDW to the continental shelves (relative to the Ctrl simulation). In general, surface freshening in the ISM simulation causes a more stratified vertical ocean structure, especially near the Antarctic continental shelf (Fig. 7). This prevents convective activity between the surface and the ocean depths, resulting in relatively colder temperatures near the surface but warmer temperatures at depth.

b. Impacts on the atmosphere

Since both the ISM and Ctrl simulations are fully coupled, the atmosphere over the Southern Ocean can be affected by ice-shelf melting and/or increased sea-ice volume. In Fig. 8, we show 30 years of annual mean 2-m air temperature, sea level pressure (SLP), and precipitation from the ISM simulation as well as differences in these quantities between the ISM and Ctrl simulations. In the Antarctic interior, the air temperature is often below -30°C, leading to a temperature gradient between the Antarctic plateau and the coastal ocean that, together with the slope of the ice sheet, lead to katabatic winds that blow from the Antarctic interior to the Southern Ocean. Precipitation over the Southern Ocean is relatively small in magnitude, with an annual average of 2–3 mm/day. The difference in precipitation between the Ctrl and ISM simulations is small (Fig. 8f). This is consistent with the observed small changed in WMT due to precipitation between the ISM and Ctrl simulations, which will be shown in Section 5. Fig. 8d shows significant coastal cooling only in the western Ross Sea and close to the Filchner Ice Shelf, with offshore cooling in the Dronning Maud Land sector. In both the Amundsen/Bellingshausen sector and over broad regions of Eastern Antarctica, there is no significant differences in 2-m air temperature either at coast or on the Plateau, meaning that the strength of katabatic winds is largely unaffected. According to geostrophic balance, the climatological winds are westerlies on the equator side of the low pressure

Accepted for publication in *Journal of Climate*. DOI 10.1175/JCLI-D-19-0683.1.

belt (50°S) and easterlies on the polar side, especially along the Antarctic coast (Fig. 8b). From the SLP differences between ISM and Ctrl (Fig. 8e), the anomalies in pressure gradient over East Antarctica show enhanced easterlies in the ISM simulation. However, along the coasts of West Antarctica, the gradients in SLP are reduced, leading to weakened coastal easterlies. Similarly, in regions of westerly winds over the western Southern Ocean, especially over the Amundsen and Bellingshausen Seas and near the Weddell Sea, the westerlies are reduced. Even with the weakened easterlies and westerlies, the Southern Ocean is colder than the Ctrl simulation, leading to more sea-ice production. The pattern of decreased 2-m air temperature is similar to the pattern of increased sea-ice concentration (Fig. 8d vs. Fig. 9a), suggesting that increased sea-ice area may cause 2-m air temperature to decrease, or vice versa.

c. Impacts on sea ice

To investigate the impacts on sea ice over the Southern Ocean, we examine the differences in mean annual sea-ice concentration, thickness, and sea-ice to ocean freshwater flux between the Ctrl and ISM simulations (Fig. 9). Sea ice concentration in the ISM simulation has increased by an area average of 5% and the sea-ice thickness has increased by about 15 cm over the Southern Ocean (Fig. 9a, b), compared to the Ctrl simulation. Merino et al. (2018) and Jourdain et al. (2017) found thinner sea ice in the Amundsen Sea with more ice-shelf melting, in contrast to our simulations with E3SM (see Fig. 9a). This is likely because of the relatively low resolution of E3SM and biases in sub-surface temperature in the Amundsen Sea in the E3SM simulations. Further, we find that more freezing occurs in the ISM than the Ctrl simulation (Fig. 9c) and that spatial patterns of these differences are similar to those for sea-ice concentration and thickness (Fig. 9a and b). The ISM simulation shows a similar sea-ice expansion as discussed by Bintanja et al. (2013), who argued that the overall increase in observed sea-ice concentration is dominated by increased ice-

Accepted for publication in *Journal of Climate*. DOI 10.1175/JCLI-D-19-0683.1.

shelf melting. Increasing sea-ice thickness in the ISM is also consistent with previous results by Hellmer (2004) and Kusahara and Hasumi (2014), who performed numerical experiments with and without ice-shelf interaction and investigated the impacts on the sea-ice distribution. As suggested by Bintanja et al. (2013), ice-shelf melting freshens the surface, which reduces convective activity between the fresh surface and the warmer subsurface layers. This cools the upper ocean, which, along with fresher surface waters, encourages more sea-ice formation (here, at an average rate of -0.05 m/yr; Fig. 9c). Bintanja et al. (2013) did not mention the air-temperature changes from their experiments, instead only arguing that there is no relationship between sea ice expansion and atmospheric variability such as the Southern Annular Mode (SAM) or stratospheric ozone. We find, however, that air temperature has also been changed in the ISM simulation compared to the Ctrl simulation, which might be directly related to increased sea-ice extent and volume.

5. Surface-flux driven water mass transformation and formation from ice-shelf melting

a. Water mass transformation

We show the annual mean WMT rate from the Ctrl and ISM simulations in Fig. 10. Broadly speaking, there are no significant differences in WMT rates due to the total surface fluxes, which are a summation of surface heat and freshwater fluxes (black lines in Fig. 10a). We do, however, find important differences in the individual components; if we further separate the WMT rate into that caused by distinct sources of freshwater flux (Fig. 10b), we see compensating differences in transformation rate between the Ctrl and ISM simulations for each source. First, freshwater flux from ice-shelf melting induces a more negative transformation rate (increased buoyancy gain) by as much as -1.74 Sv (peaking at a neutral density of 27.4 $\mathrm{kg\,m^{-3}}$) compared to the Ctrl simulation. Second, ice-shelf melting also has a significant, indirect effect on sea ice. The transformation rate

Accepted for publication in *Journal of Climate*. DOI 10.1175/JCLI-D-19-0683.1.

due to sea-ice formation and melting increases by as much as 1.79 Sv, at the same high density levels affected by ice-shelf melting, but decreases by -0.84 Sv at lower densities (with the largest decrease at 26.4 $\mathrm{kg\,m^{-3}}$). Third, we find no notable changes in the transformation rate by freshwater fluxes from the atmosphere and land (E-P-R term) between the two simulations. Meanwhile, there is no AABW formation in either the Ctrl or ISM simulations and transformation rates of LCDW in the two simulations are minimal. Formation of AABW is notably difficult to represent in low resolution of general circulation models (Aguiar et al. 2017). In addition, most CMIP5 models have temperature and salinity biases over the entire water column in Southern Ocean, which is a factor influencing the density of seawater (Sallée et al. 2013). Both Ctrl and ISM simulations have such temperature and salinity biases in the Southern Ocean as shown in Fig. 2.

In Fig. 11, we plot the climatological annual cycle of WMT rate caused by freshwater fluxes from sea-ice formation and melting and from ice-shelf melting. Consistent with Fig. 10, ice-shelf melting always produces a negative transformation rate (Fig. 11b), regardless of the season, at a neutral density of approximately 27.4 $\mathrm{kg\,m^{-3}}$. In contrast, the transformation caused by sea-ice formation and melting has large seasonal variability (Fig. 11a), with a positive transformation rate (buoyancy loss) during the winter and a negative transformation rate (buoyancy gain) during the summer. These differences in transformation rate between the two simulations (Fig. 11c) show that the ISM simulation has an overall stronger seasonal sea-ice cycle. During winter, the ISM simulation has a more positive transformation rate due to sea-ice formation, peaking at a neutral density of 27.4 $\mathrm{kg\,m^{-3}}$ where ice-shelf melting is also influential. During summer, the ISM simulation has a more negative transformation rate due to sea-ice melting at lower density levels, which compensates for the more positive transformation rate in winter.

Accepted for publication in *Journal of Climate*. DOI 10.1175/JCLI-D-19-0683.1.

b. Water mass formation

Finally, we investigate how ice-shelf melting and sea-ice formation and melting impact water mass formation and destruction by decomposing the water mass formation rate into contributions from different surface flux processes (Fig. 12). The water mass formation rate is the difference of the WMT rate with respect to density and represents volume convergence (for positive values, corresponding to downwelling) or divergence (for negative values, corresponding to upwelling) within a particular density range (Abernathey et al. 2016). The freshwater flux from ice-shelf melting can thus indirectly impact the water mass formation rate through sea-ice formation and melting (Fig. 12a). For both the Ctrl and ISM simulation, the combined effects of sea-ice formation and melting destroy a considerable amount of water mass (corresponding to a negative formation rate) in the density range from $26.4\,\mathrm{kg\,m^{-3}}$ to $27.4\,\mathrm{kg\,m^{-3}}$ (Surface Water). Yet there is additional water mass destruction in this same density range by as much as 2.57 Sv for the ISM simulation (Table 5). The freshwater flux from ice-shelf melting directly induces transformation (corresponding to a negative formation rate) at relatively high-density levels (UCDW and LCDW) and this upwelled water is directly converted to lower densities (Fig. 12b). The total amount of upwelling due to ice-shelf melting is approximately 1.77 Sv (Table 5). Fig. 12c-f shows the WMF rate for the Southern Ocean divided into the Amery ice-shelf sector, Ross Sea, Amundsen Sea and Weddell Sea sectors. It is evident that the Amery ice-shelf sector dominates the WMF rate, and that upwelled water here is converted to relatively low densities. This is probably due to relatively warm water coming up onto the continental shelf in the Amery ice-shelf sector in the ISM simulation (Fig. 6g), and thus melt rates are probably too high compared to Rignot et al. (2013) (e.g., note large melt biases in Dronning Maud Land region and for the Amery Ice Shelf in Fig. 1). The Indian Ocean sector (the Dronning Maud Land region of Antarctica) has a particularly narrow

Accepted for publication in *Journal of Climate*. DOI 10.1175/JCLI-D-19-0683.1.

continental shelf, and the model resolution is likely insufficient to separate warmer water in the deeper Weddell Sea from colder water trapped on the continental shelf.

6. Summary and conclusions

By comparing otherwise identical Earth system model simulations with and without ice-shelf melt fluxes we have used E3SM to characterize and quantify the impacts of ice-shelf melting and freezing processes on WMT and WMF. We find no significant differences in net Southern Ocean WMT due to the differences in total surface fluxes between the two simulations. Yet, when we separate the WMT rate into its constituent processes, we find important differences in both WMT and WMF rate between the simulations. Meltwater from ice shelves makes Surface Water and UCDW water masses in the Southern Ocean lighter (corresponding to a buoyancy gain) at relatively high density values. Meanwhile, the freshwater flux from sea-ice formation makes these water masses denser (corresponding to a buoyancy loss) at these same high density values. Effectively, ice-shelf meltwater is partially counteracting the densification of seawater from brine rejection at these densities, with even more of a cancellation likely under future climate scenarios in which ice-shelf melting is likely to increase. Ice-shelf melting produces transformation of UCDW water masses at relatively high density values where ice-shelf melting is dominant and this upwelled water is directly converted to lower density values. Freshwater fluxes produced by ice-shelf melting have a further, indirect impact on the Southern Ocean overturning circulation through the action of increased sea-ice formation, which also cause considerable upwelling and effectively further amplifies the overturning that occurs from the buoyancy of ice-shelf meltwater directly. Importantly, we find that this indirect impact is larger than the direct impact.

We have found that surface freshening by ice-shelf melting increases density stratification near the Antarctic coast and hence reduces vertical heat transport from the deeper ocean, trapping

Accepted for publication in *Journal of Climate*. DOI 10.1175/JCLI-D-19-0683.1.

warmer water at depth. In some regions, this trapped heat might be expected to reach ice-shelf cavities through changes in ocean currents and/or density structure in future climate scenarios (Hellmer et al. 2012). Indeed, in some regions of Antarctica, feedbacks between ice-shelf melting and trapping of warmer waters have already been observed (Silvano et al. 2018). This more stratified ocean makes the sea surface colder, which along with the additional freshwater, results in significant Antarctic sea-ice expansion in simulations that include ice shelf melt fluxes. In addition, we have also found that air temperature has decreased in the ISM simulation compared to the Ctrl simulation, which may be directly related to sea-ice expansion. As air temperatures decrease, the sea ice is likely to increase even further in a feedback. Our model configuration does not allow us to investigate the trends of Antarctic sea-ice but rather the mean state of sea-ice with ice-shelf melting and, as stated previously, the change in freshwater flux between our ISM and Ctrl simulations is an order of magnitude larger than the observed trend in freshwater input (Bamber et al. 2018). With these caveats, our findings of sea-ice expansion by ice-shelf melting are consistent with the proposal that increased ice-shelf melting over the past decades (e.g., Shepherd et al. 2004; Pritchard et al. 2012; Khazendar et al. 2016) could be a cause for the observed sea-ice expansion over that same time period.

Abernathey et al. (2016) assessed the relative contributions of sea-ice freezing and melting, together with other modes of air-sea interaction, to Southern Ocean overturning and revealed the central role of sea-ice formation and melting in transforming upwelled Circumpolar Deep Water. Although we found no significant changes to those conclusions in this study, our results do show that the addition of ice-shelf melting to Earth system models increases the importance of sea-ice in Southern Ocean overturning. In other words, the increase in Antarctic ice-shelf melting over the historical time period (Shepherd et al. 2004; Pritchard et al. 2012; Khazendar et al. 2016; Holland et al. 2019) has likely increased the role of sea-ice in Southern Ocean overturning.

Accepted for publication in *Journal of Climate*. DOI 10.1175/JCLI-D-19-0683.1.

Silvano et al. (2018) suggested that increased glacial melt water will reduce AABW formation by offsetting increased salt flux during sea-ice formation in coastal polynyas. These effects would then prevent full-depth convection and the formation of dense shelf water. In this study we have used a relatively low resolution version of E3SM, which does not have a good representation of Antarctic coastal polynyas. This may explain why we do not find changes in dense water formation related to ice-shelf melting. Future E3SM studies will investigate the impacts of ice-shelf melting and the inclusion of ice-shelf cavities at higher resolution.

Whereas Bintanja et al. (2013) put freshwater fluxes from ice-shelf melting at the ocean surface, our ISM simulation places that freshwater at the depth of the ice-shelf base, inducing overturning that may either enhance or suppress local sea-ice formation, depending on deeper ocean conditions (Donat-Magnin et al. 2017; Jourdain et al. 2017; Mathiot et al. 2017). In addition, ice-shelf melting is not uniform along the Antarctic coast (Rignot et al. 2013; Depoorter et al. 2013), suggesting the possibility for strong regional variation in how ice shelf melting affects sea ice. Care must be taken in how Antarctic ice-shelf melt is distributed along the coast in global coupled climate simulations. Here, prognostic basal melt fluxes from individually modeled ice shelves influence and are, in turn, influenced by regional differences in sea-ice expansion and WMT. In that sense, the E3SM model used here captures the important features mentioned above. As highlighted by our results, fully coupled models including ice sheets, such as planned for future versions of E3SM, are required for investigating potential feedbacks between Antarctic ice-shelves and ocean and sea-ice properties.

While this study only considers the impacts of ice-shelf melting on the Southern Ocean, iceberg melting represents approximately half of the mass flux from the Antarctic ice sheet to the ocean (Rignot et al. 2013; Depoorter et al. 2013). Calved icebergs transport freshwater away from the Antarctic coast and exchange heat with the ocean, thereby affecting ocean stratification and circulation, with subsequent indirect thermodynamic effects on the sea-ice system (Hunke and Comeau

Accepted for publication in *Journal of Climate*. DOI 10.1175/JCLI-D-19-0683.1.

2011; Stern et al. 2016; Merino et al. 2016). Future work to address these effects should include a comprehensive analysis considering the impacts of both melting from ice shelves and calved icebergs.

Acknowledgments. This research was supported by the Energy Exascale Earth System Model (E3SM) project, funded by the U.S. Department of Energy Office of Science, Biological and Environmental Research program. E3SM simulations used computing resources from the Argonne Leadership Computing Facility (U.S. DOE contract DE-AC02-06CH11357), the National Energy Research Scientific Computing Center (U.S. DOE contract DE-AC02-05CH11231), and the Oak Ridge Leadership Computing Facility at the Oak Ridge National Laboratory (U.S. DOE contract DE-AC05-00OR22725), awarded under an ASCR Leadership Computing Challenge (ALCC) award. R. Abernathey acknowledges support from NSF award OCE-1553593. M. Mazloff acknowledges support from NSF grants OCE-1658001, OCE-1924388, and PLR-1425989. The authors appreciate three anonymous reviewers.

References

Abernathey, R., I. Cerovecki, P. Holland, E. Newsom, M. Mazloff, and L. Talley, 2016: Water-mass transformation by sea ice in the upper branch of the Southern Ocean overturning. *Nature Geoscience*, **9 (8)**, 596.

Aguiar, W., M. M. Mata, and R. Kerr, 2017: On deep convection events and antarctic bottom water formation in ocean reanalysis products. *Ocean Science*, **13 (6)**.

Bamber, J. L., R. M. Westaway, B. Marzeion, and B. Wouters, 2018: The land ice contribution to sea level during the satellite era. *Environmental Research Letters*, **13 (6)**, 063 008, doi:10.1088/1748-9326/aac2f0.

Accepted for publication in *Journal of Climate*. DOI 10.1175/JCLI-D-19-0683.1.

Bintanja, R., G. J. Van Oldenborgh, S. S. Drijfhout, B. Wouters, and C. A. Katsman, 2013: Important role for ocean warming and increased ice-shelf melt in Antarctic sea-ice expansion. *Nature Geoscience*, **6 (5)**, 376.

Bitz, C., and L. M. Polvani, 2012: Antarctic climate response to stratospheric ozone depletion in a fine resolution ocean climate model. *Geophysical Research Letters*, **39 (20)**.

Bracegirdle, T. J., E. Shuckburgh, J.-B. Sallee, Z. Wang, A. J. Meijers, N. Bruneau, T. Phillips, and L. J. Wilcox, 2013: Assessment of surface winds over the atlantic, indian, and pacific ocean sectors of the southern ocean in cmip5 models: Historical bias, forcing response, and state dependence. *Journal of Geophysical Research: Atmospheres*, **118 (2)**, 547–562.

Briegleb, B. P., G. Danabasoglu, and W. G. Large, 2010: An Overflow parameterization for the ocean component of the Community Climate System Model. Tech. Rep. NCAR/TN-481+STR, NCAR. doi:10.5065/D69K4863.

Cavalieri, D., C. Parkinson, P. Gloersen, and H. Zwally, 1996: updated yearly: Sea ice concentrations from nimbus-7 smmr and dmsp ssm/i-ssmis passive microwave data (1981-2011). *National Snow and Ice Data Center, Boulder, CO, digital media.[Available online at doi: 10.5067/8GQ8LZQVL0VL.]*.

Comiso, J., 1999: Bootstrap sea ice concentrations for nimbus-7 smmr and dmsp ssm/i. *Digital Media, National Snow and Ice Data Center*, **10**, J6JQLS9EJ5HU.

Cunningham, S., S. Alderson, B. King, and M. Brandon, 2003: Transport and variability of the antarctic circumpolar current in drake passage. *Journal of Geophysical Research: Oceans*, **108 (C5)**.

Accepted for publication in *Journal of Climate*. DOI 10.1175/JCLI-D-19-0683.1.

Dansereau, V., P. Heimbach, and M. Losch, 2014: Simulation of subice shelf melt rates in a general circulation model: Velocity-dependent transfer and the role of friction. *Journal of Geophysical Research: Oceans*, **119 (3)**, 1765–1790, doi:10.1002/2013JC008846.

De Lavergne, C., G. Madec, J. Le Sommer, A. G. Nurser, and A. C. Naveira Garabato, 2016: On the consumption of antarctic bottom water in the abyssal ocean. *Journal of Physical Oceanography*, **46 (2)**, 635–661.

Depoorter, M. A., J. Bamber, J. Griggs, J. T. Lenaerts, S. R. Ligtenberg, M. R. van den Broeke, and G. Moholdt, 2013: Calving fluxes and basal melt rates of antarctic ice shelves. *Nature*, **502 (7469)**, 89.

Donat-Magnin, M., N. C. Jourdain, P. Spence, J. Le Sommer, H. Gallée, and G. Durand, 2017: Ice-shelf melt response to changing winds and glacier dynamics in the amundsen sea sector, antarctica. *Journal of Geophysical Research: Oceans*, **122 (12)**, 10 206–10 224.

Donohue, K., K. Tracey, D. Watts, M. P. Chidichimo, and T. Chereskin, 2016: Mean antarctic circumpolar current transport measured in drake passage. *Geophysical Research Letters*, **43 (22)**, 11–760.

Eyring, V., S. Bony, G. A. Meehl, C. A. Senior, B. Stevens, R. J. Stouffer, and K. E. Taylor, 2016: Overview of the coupled model intercomparison project phase 6 (cmip6) experimental design and organization. *Geoscientific Model Development (Online)*, **9 (LLNL-JRNL-736881)**.

Flato, G., and Coauthors, 2013: Evaluation of climate models. Cambridge University Press.

Golaz, J.-C., and Coauthors, 2019: The DOE E3SM coupled model version 1: Overview and evaluation at standard resolution. *Journal of Advances in Modeling Earth Systems*,

Accepted for publication in *Journal of Climate*. DOI 10.1175/JCLI-D-19-0683.1.

602 **11 (ja)**, doi:10.1029/2018MS001603, URL https://agupubs.onlinelibrary.wiley.com/doi/abs/10.
603 1029/2018MS001603.

604 Good, S. A., M. J. Martin, and N. A. Rayner, 2013: En4: Quality controlled ocean tempera-
605 ture and salinity profiles and monthly objective analyses with uncertainty estimates. *Journal of*
606 *Geophysical Research: Oceans*, **118 (12)**, 6704–6716.

607 Gouretski, V., 2018: Woce-argo global hydrographic climatology (waghc version 1.0), world data
608 center for climate (wdcc) at dkrz. World Data Center for Climate (WDCC) at DKRZ.

609 Groeskamp, S., R. P. Abernathey, and A. Klocker, 2016: Water mass transformation by cabbeling
610 and thermobaricity. *Geophysical Research Letters*, **43 (20)**, 10–835.

611 Hellmer, H. H., 2004: Impact of antarctic ice shelf basal melting on sea ice and deep ocean
612 properties. *Geophysical Research Letters*, **31 (10)**.

613 Hellmer, H. H., F. Kauker, R. Timmermann, J. Determann, and J. Rae, 2012: Twenty-first-century
614 warming of a large antarctic ice-shelf cavity by a redirected coastal current. *Nature*, **485 (7397)**,
615 225.

616 Hellmer, H. H., and D. J. Olbers, 1989: A two-dimensional model for the thermohaline circulation
617 under an ice shelf. *Antarctic Science*, **1 (4)**, 325–336.

618 Heuzé, C., K. J. Heywood, D. P. Stevens, and J. K. Ridley, 2013: Southern ocean bottom water
619 characteristics in cmip5 models. *Geophysical Research Letters*, **40 (7)**, 1409–1414.

620 Holland, D. M., and A. Jenkins, 1999: Modeling Thermodynamic Ice–Ocean Interactions
621 at the Base of an Ice Shelf. *Journal of Physical Oceanography*, **29 (8)**, 1787–1800, doi:
622 10.1175/1520-0485(1999)029⟨1787:MTIOIA⟩2.0.CO;2, URL http://journals.ametsoc.org/doi/
623 abs/10.1175/1520-0485(1999)029%3C1787:MTIOIA%3E2.0.CO;2.

Accepted for publication in *Journal of Climate*. DOI 10.1175/JCLI-D-19-0683.1.

Holland, P. R., T. J. Bracegirdle, P. Dutrieux, A. Jenkins, and E. J. Steig, 2019: West Antarctic ice loss influenced by internal climate variability and anthropogenic forcing. *Nature Geoscience*, **12**, 718–724, doi:10.1038/s41561-019-0420-9.

Hunke, E. C., and D. Comeau, 2011: Sea ice and iceberg dynamic interaction. *Journal of Geophysical Research: Oceans*, **116 (5)**, 1–9, doi:10.1029/2010JC006588.

Jackett, D. R., and T. J. McDougall, 1997: A neutral density variable for the world's oceans. *Journal of Physical Oceanography*, **27 (2)**, 237–263.

Jacobs, S. S., and C. F. Giulivi, 2010: Large multidecadal salinity trends near the Pacific–Antarctic continental margin. *Journal of Climate*, **23 (17)**, 4508–4524.

Jacobs, S. S., C. F. Giulivi, and P. A. Mele, 2002: Freshening of the Ross Sea during the late 20th century. *Science*, **297 (5580)**, 386–389.

Jenkins, A., K. W. Nicholls, and H. F. Corr, 2010: Observation and parameterization of ablation at the base of Ronne Ice Shelf, Antarctica. *Journal of Physical Oceanography*, **40 (10)**, 2298–2312, doi:10.1175/2010JPO4317.1.

Jourdain, N. C., P. Mathiot, N. Merino, G. Durand, J. Le Sommer, P. Spence, P. Dutrieux, and G. Madec, 2017: Ocean circulation and sea-ice thinning induced by melting ice shelves in the a mundsen s ea. *Journal of Geophysical Research: Oceans*, **122 (3)**, 2550–2573.

Kalnay, E., and Coauthors, 1996: The ncep/ncar 40-year reanalysis project. *Bulletin of the American meteorological Society*, **77 (3)**, 437–472.

Khazendar, A., and Coauthors, 2016: Rapid submarine ice melting in the grounding zones of ice shelves in West Antarctica. *Nature Communications*, **7**, 13 243–13 243, doi:10.1038/ncomms13243.

Accepted for publication in *Journal of Climate*. DOI 10.1175/JCLI-D-19-0683.1.

Klocker, A., T. J. McDougall, and D. R. Jackett, 2009: A new method for forming approximately neutral surfaces. *Ocean Science*, **5 (2)**, 155–172.

Kurtz, N., and T. Markus, 2012: Satellite observations of antarctic sea ice thickness and volume. *Journal of Geophysical Research: Oceans*, **117 (C8)**.

Kusahara, K., and H. Hasumi, 2014: Pathways of basal meltwater from antarctic ice shelves: A model study. *Journal of Geophysical Research: Oceans*, **119 (9)**, 5690–5704.

Kwok, R., J. Comiso, T. Lee, and P. Holland, 2016: Linked trends in the South Pacific sea ice edge and Southern Oscillation Index. *Geophysical Research Letters*, **43 (19)**, 10–295.

Li, X., D. M. Holland, E. P. Gerber, and C. Yoo, 2014: Impacts of the north and tropical atlantic ocean on the antarctic peninsula and sea ice. *Nature*, **505 (7484)**, 538.

Locarnini, R., and Coauthors, 2018: World ocean atlas 2018, volume 1: Temperature. Mishonov Technical Ed.

Marshall, J., and K. Speer, 2012: Closure of the meridional overturning circulation through Southern Ocean upwelling. *Nature Geoscience*, **5 (3)**, 171.

Mathiot, P., A. Jenkins, C. Harris, and G. Madec, 2017: Explicit representation and parametrised impacts of under ice shelf seas in the z * coordinate ocean model nemo 3.6, geosci. model dev., 10, 2849–2874. gmd-10-2849-2017.

Mazloff, M. R., P. Heimbach, and C. Wunsch, 2010: An eddy-permitting Southern Ocean state estimate. *Journal of Physical Oceanography*, **40 (5)**, 880–899.

Menary, M. B., and Coauthors, 2018: Preindustrial control simulations with hadgem3-gc3. 1 for cmip6. *Journal of Advances in Modeling Earth Systems*, **10 (12)**, 3049–3075.

Accepted for publication in *Journal of Climate*. DOI 10.1175/JCLI-D-19-0683.1.

Merino, N., N. C. Jourdain, J. Le Sommer, H. Goosse, P. Mathiot, and G. Durand, 2018: Impact of increasing Antarctic glacial freshwater release on regional sea-ice cover in the Southern Ocean. *Ocean Modelling*, **121**, 76–89.

Merino, N., J. Le Sommer, G. Durand, N. C. Jourdain, G. Madec, P. Mathiot, and J. Tournadre, 2016: Antarctic icebergs melt over the Southern Ocean: Climatology and impact on sea ice. *Ocean Modelling*, **104**, 99–110.

Montgomery, R. B., 1958: Water characteristics of Atlantic Ocean and of world ocean. *Deep Sea Research (1953)*, **5 (2-4)**, 134–148.

Morrison, A. K., A. M. Hogg, and M. L. Ward, 2011: Sensitivity of the southern ocean overturning circulation to surface buoyancy forcing. *Geophysical research letters*, **38 (14)**.

Parkinson, C. L., 2019: A 40-y record reveals gradual antarctic sea ice increases followed by decreases at rates far exceeding the rates seen in the arctic. *Proceedings of the National Academy of Sciences*, 201906556.

Petersen, M. R., D. W. Jacobsen, T. D. Ringler, M. W. Hecht, and M. E. Maltrud, 2015: Evaluation of the arbitrary Lagrangian-Eulerian vertical coordinate method in the MPAS-Ocean model. *Ocean Modelling*, **86 (0)**, 93 – 113, doi:http://dx.doi.org/10.1016/j.ocemod.2014.12.004, URL http://www.sciencedirect.com/science/article/pii/S1463500314001796.

Petersen, M. R., and Coauthors, 2019: An evaluation of the ocean and sea ice climate of e3sm using mpas and interannual core-ii forcing. *Journal of Advances in Modeling Earth Systems*, **11 (5)**, 1438–1458, doi:10.1029/2018MS001373, URL https://agupubs.onlinelibrary.wiley.com/doi/abs/10.1029/2018MS001373, https://agupubs.onlinelibrary.wiley.com/doi/pdf/10.1029/2018MS001373.

Accepted for publication in *Journal of Climate*. DOI 10.1175/JCLI-D-19-0683.1.

Pritchard, H. D., S. R. M. Ligtenberg, H. a. Fricker, D. G. Vaughan, M. R. van den Broeke, and L. Padman, 2012: Antarctic ice-sheet loss driven by basal melting of ice shelves. *Nature*, **484 (7395)**, 502–505, doi:10.1038/nature10968.

Qian, Y., and Coauthors, 2018: Parametric sensitivity and uncertainty quantification in the version 1 of E3SM Atmosphere Model based on short perturbed parameter ensemble simulations. *Journal of Geophysical Research: Atmospheres*, **123 (23)**, 13–046.

Rasch, P., and Coauthors, 2019: An overview of the atmospheric component of the energy exascale earth system model. *Journal of Advances in Modeling Earth Systems*, doi:10.1029/2019MS001629.

Reckinger, S. M., M. R. Petersen, and S. J. Reckinger, 2015: A study of overflow simulations using mpas-ocean: Vertical grids, resolution, and viscosity. *Ocean Modelling*, **96, Part 2**, 291 – 313, doi:http://dx.doi.org/10.1016/j.ocemod.2015.09.006, URL http://www.sciencedirect.com/science/article/pii/S146350031500164X.

Rignot, E., S. Jacobs, J. Mouginot, and B. Scheuchl, 2013: Ice-shelf melting around antarctica. *Science*, **341 (6143)**, 266–270.

Ringler, T., M. Petersen, R. Higdon, D. Jacobsen, P. Jones, and M. Maltrud, 2013: A multi-resolution approach to global ocean modeling. *Ocean Modelling*, **69 (0)**, 211–232, doi:http://dx.doi.org/10.1016/j.ocemod.2013.04.010, URL http://www.sciencedirect.com/science/article/pii/S1463500313000760.

Roemmich, D., J. Church, J. Gilson, D. Monselesan, P. Sutton, and S. Wijffels, 2015: Unabated planetary warming and its ocean structure since 2006. *Nature climate change*, **5 (3)**, 240.

Accepted for publication in *Journal of Climate*. DOI 10.1175/JCLI-D-19-0683.1.

Sallée, J.-B., R. J. Matear, S. R. Rintoul, and A. Lenton, 2012: Localized subduction of anthropogenic carbon dioxide in the Southern Hemisphere oceans. *Nature Geoscience*, **5 (8)**, 579.

Sallée, J.-B., E. Shuckburgh, N. Bruneau, A. J. Meijers, T. J. Bracegirdle, Z. Wang, and T. Roy, 2013: Assessment of southern ocean water mass circulation and characteristics in cmip5 models: Historical bias and forcing response. *Journal of Geophysical Research: Oceans*, **118 (4)**, 1830–1844.

Séférian, R., D. Iudicone, L. Bopp, T. Roy, and G. Madec, 2012: Water mass analysis of effect of climate change on air–sea co2 fluxes: The southern ocean. *Journal of climate*, **25 (11)**, 3894–3908.

Shepherd, A., D. Wingham, and E. Rignot, 2004: Warm ocean is eroding West Antarctic Ice Sheet. *Geophysical Research Letters*, **31 (23)**, L23 402, doi:10.1029/2004GL021106.

Sigmond, M., and J. C. Fyfe, 2010: Has the ozone hole contributed to increased Antarctic sea ice extent? *Geophysical Research Letters*, **37 (18)**.

Silvano, A., S. R. Rintoul, B. Peña-Molino, W. R. Hobbs, E. van Wijk, S. Aoki, T. Tamura, and G. D. Williams, 2018: Freshening by glacial meltwater enhances melting of ice shelves and reduces formation of antarctic bottom water. *Science advances*, **4 (4)**, eaap9467.

Speer, K., S. R. Rintoul, and B. Sloyan, 2000: The diabatic Deacon cell. *Journal of physical oceanography*, **30 (12)**, 3212–3222.

Stammerjohn, S., D. Martinson, R. Smith, X. Yuan, and D. Rind, 2008: Trends in Antarctic annual sea ice retreat and advance and their relation to El Niño–Southern Oscillation and Southern Annular Mode variability. *Journal of Geophysical Research: Oceans*, **113 (C3)**.

Accepted for publication in *Journal of Climate*. DOI 10.1175/JCLI-D-19-0683.1.

731 Stern, A., A. Adcroft, and O. Sergienko, 2016: The effects of Antarctic iceberg calving-size dis-
732 tribution in a global climate model. *Journal of Geophysical Research: Oceans*, **121 (8)**, 5773–
733 5788.

734 Thompson, D. W., S. Solomon, P. J. Kushner, M. H. England, K. M. Grise, and D. J. Karoly, 2011:
735 Signatures of the Antarctic ozone hole in Southern Hemisphere surface climate change. *Nature*
736 *geoscience*, **4 (11)**, 741.

737 Thomson, R. E., and W. J. Emery, 2014: *Data analysis methods in physical oceanography*.
738 Newnes.

739 Turner, J., T. J. Bracegirdle, T. Phillips, G. J. Marshall, and J. S. Hosking, 2013: An initial assess-
740 ment of Antarctic sea ice extent in the CMIP5 models. *Journal of Climate*, **26 (5)**, 1473–1484.

741 Turner, J., and Coauthors, 2009: Non-annular atmospheric circulation change induced by strato-
742 spheric ozone depletion and its role in the recent increase of Antarctic sea ice extent. *Geophys-*
743 *ical Research Letters*, **36 (8)**.

744 Walin, G., 1982: On the relation between sea-surface heat flow and thermal circulation in the
745 ocean. *Tellus*, **34 (2)**, 187–195.

746 Whitworth, T., and R. Peterson, 1985: Volume transport of the antarctic circumpolar current from
747 bottom pressure measurements. *Journal of Physical Oceanography*, **15 (6)**, 810–816.

748 Xie, S., and Coauthors, 2018: Understanding cloud and convective characteristics in version 1
749 of the E3SM Atmosphere Model. *Journal of Advances in Modeling Earth Systems*, **10 (10)**,
750 2618–2644.

751 Zhang, J., 2007: Increasing Antarctic sea ice under warming atmospheric and oceanic conditions.
752 *Journal of Climate*, **20 (11)**, 2515–2529.

Accepted for publication in *Journal of Climate*. DOI 10.1175/JCLI-D-19-0683.1.

753 Zhang, L., T. L. Delworth, W. Cooke, and X. Yang, 2019: Natural variability of southern ocean
754 convection as a driver of observed climate trends. *Nature Climate Change*, **9 (1)**, 59.

Accepted for publication in *Journal of Climate*. DOI 10.1175/JCLI-D-19-0683.1.

LIST OF TABLES

Accepted for publication in *Journal of Climate*. DOI 10.1175/JCLI-D-19-0683.1.

771 TABLE 1. Antarctic freshwater fluxes to the ocean for each simulation, averaged over last 15 years. Standard
772 deviations are in parentheses. The runoff term includes a solid ice (excess snow from snowcapping) and liquid
773 (rain) term, determined by precipitation over Antarctica. The ISM simulation has an additional freshwater term
774 from explicit ice-shelf melt fluxes, adding about 50% to the total Antarctic runoff over Ctrl.

	Ctrl	ISM
Runoff	0.087 (0.042) Sv	0.080 (0.041) Sv
Ice-shelf melting	0 Sv	0.045 (0.003) Sv
Total	0.087 (0.042) Sv	0.125 (0.041) Sv

Accepted for publication in *Journal of Climate*. DOI 10.1175/JCLI-D-19-0683.1.

TABLE 2. Atmosphere, ocean and sea-ice estimation data sets used in this study.

Data sets	Variables	Periods	Reference
NCEP/NCAR Reanalysis I	Zonal wind stress	2005-2010	(Kalnay et al. 1996)
SOSE	Temperature, Salinity, Zonal and meridional components of velocity, Sea-ice to ocean freshwater flux	2005-2010	(Mazloff et al. 2010)
EN4	Temperature, Salinity	1995-2018	(Good et al. 2013)
WOA18	Temperature, Salinity	1995-2018	(Locarnini et al. 2018)
WAGHC	Temperature, Salinity	1985-2016	(Gouretski 2018)
SSM/I NASATeam	Sea-ice concentration	1979-2009	(Cavalieri et al. 1996)
ICESat	Sea-ice thickness	2003-2008	(Kurtz and Markus 2012)

Accepted for publication in *Journal of Climate*. DOI 10.1175/JCLI-D-19-0683.1.

TABLE 3. Definition of parameter in Equation 1 and 5

Parameter	Description	Units
Ω	WMT rate	Sv
M	WMF rate	Sv
σ_k	Surface-referenced potential density	$\mathrm{kg\,m^{-3}}$
t	Time	s
α	Thermal expansion	$\mathrm{kg\,m^{-3}\,K^{-1}}$
Q_{net}	Downward surface heat flux	$\mathrm{W\,m^{-2}}$
C_p	Specific heat of seawater (3,994)	$\mathrm{J\,kg^{-1}\,K^{-1}}$
β	Haline coefficient of contraction	$\mathrm{kg\,m^{-3}\,PSU^{-1}}$
F_{net}	Downward surface freshwater flux	$\mathrm{kg\,m^{-2}\,s^{-1}}$
S	Sea surface salinity	PSU
ρ_0	Constant reference density of seawater (1,035)	$\mathrm{kg\,m^{-3}}$
A	Horizontal ocean surface area of interest	$\mathrm{m^2}$

Accepted for publication in *Journal of Climate*. DOI 10.1175/JCLI-D-19-0683.1.

TABLE 4. Interpretation of WMT and formation rate.

	Positive	Negative
Transformation rates	Denser	Lighter
	Lose buoyancy	Gain buoyancy
Formation rates	Water convergence	Water divergence
	Downwelling motion	Upwelling motion

Accepted for publication in *Journal of Climate*. DOI 10.1175/JCLI-D-19-0683.1.

TABLE 5. Thirty-year annual mean of transformation anomaly caused by either freshwater flux from ice-shelf melting or from sea-ice formation and melting. Rows show results from the ISM and Ctrl simulations, and their differences. Values in parentheses represent the standard deviation over 30 years of the annual mean (indicating the level of interannual variability) of upwelled water in each simulation.

	Ice-shelf melting	Sea-ice formation and melting
ISM	-1.77 (0.12) Sv	-19.04 (1.75) Sv
Ctrl	N/A	-16.47 (1.56) Sv
ISM - Ctrl	-1.77 Sv	-2.57 Sv

Accepted for publication in *Journal of Climate*. DOI 10.1175/JCLI-D-19-0683.1.

LIST OF FIGURES

Accepted for publication in *Journal of Climate*. DOI 10.1175/JCLI-D-19-0683.1.

Accepted for publication in *Journal of Climate*. DOI 10.1175/JCLI-D-19-0683.1.

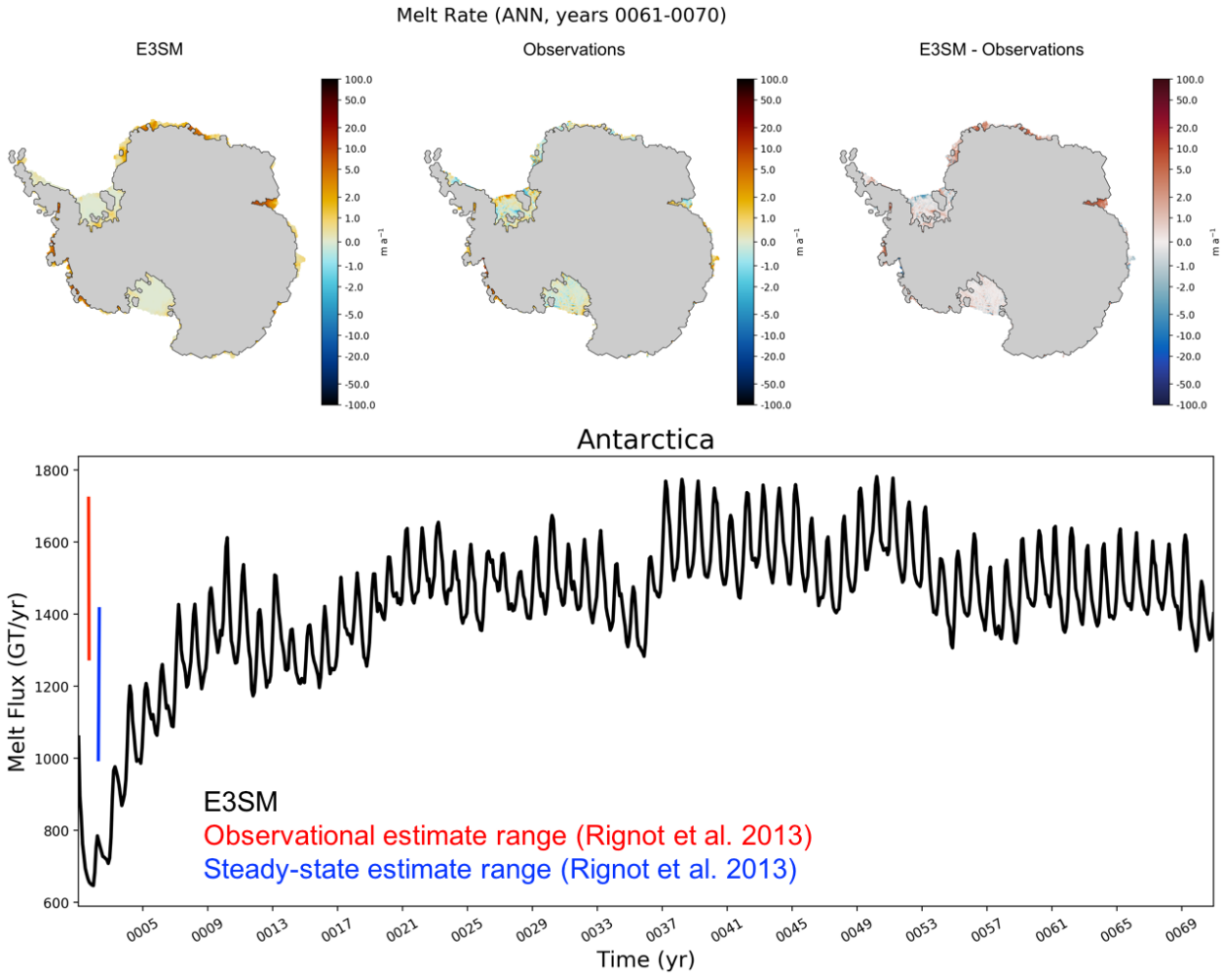

FIG. 1. Top left: melt rates (m a^{-1}) from Antarctic ice-shelves from the ISM simulation, averaged over ten years near the end of the simulation. Top middle: satellite-derived melt rates (Rignot et al. 2013). Top right: the difference between the previous panels. Each panel uses the coastline and grounding line as seen by E3SM to give the reader a sense of the resolution of the model. Bottom: A time series of the total Antarctic melt flux with present-day estimates and those inferred if the AIS were in steady state (rather than losing mass) from Rignot et al. (2013). The steady-state value may be the more appropriate comparison for pre-industrial conditions.

Accepted for publication in *Journal of Climate*. DOI 10.1175/JCLI-D-19-0683.1.

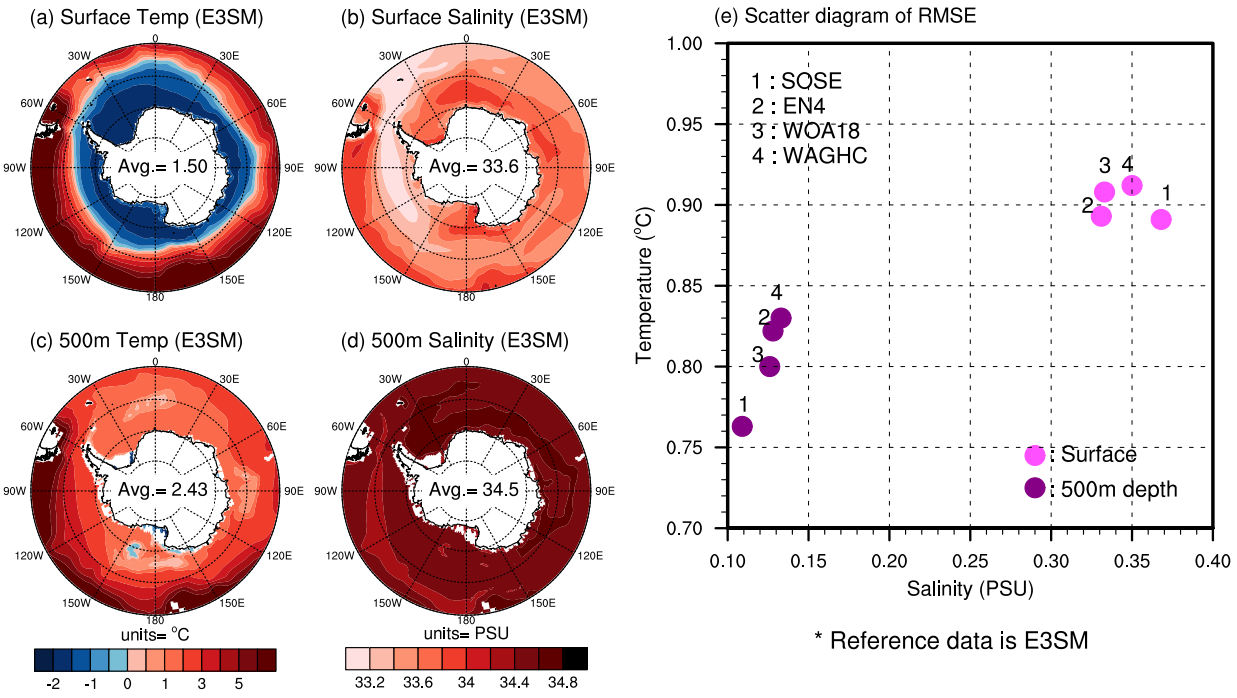

FIG. 2. Spatial distribution of annual mean sea-surface (a) temperature, (b) salinity; 500 m depth (c) temperature, (d) salinity from E3SM (30-year average from the Ctrl simulation); and (e) scatter diagram of RMSE (root mean square error) for sea-surface and 500 m depth temperature and salinity between E3SM and four ocean products from SOSE, EN4, WOA18, and WAGHC.

Accepted for publication in *Journal of Climate*. DOI 10.1175/JCLI-D-19-0683.1.

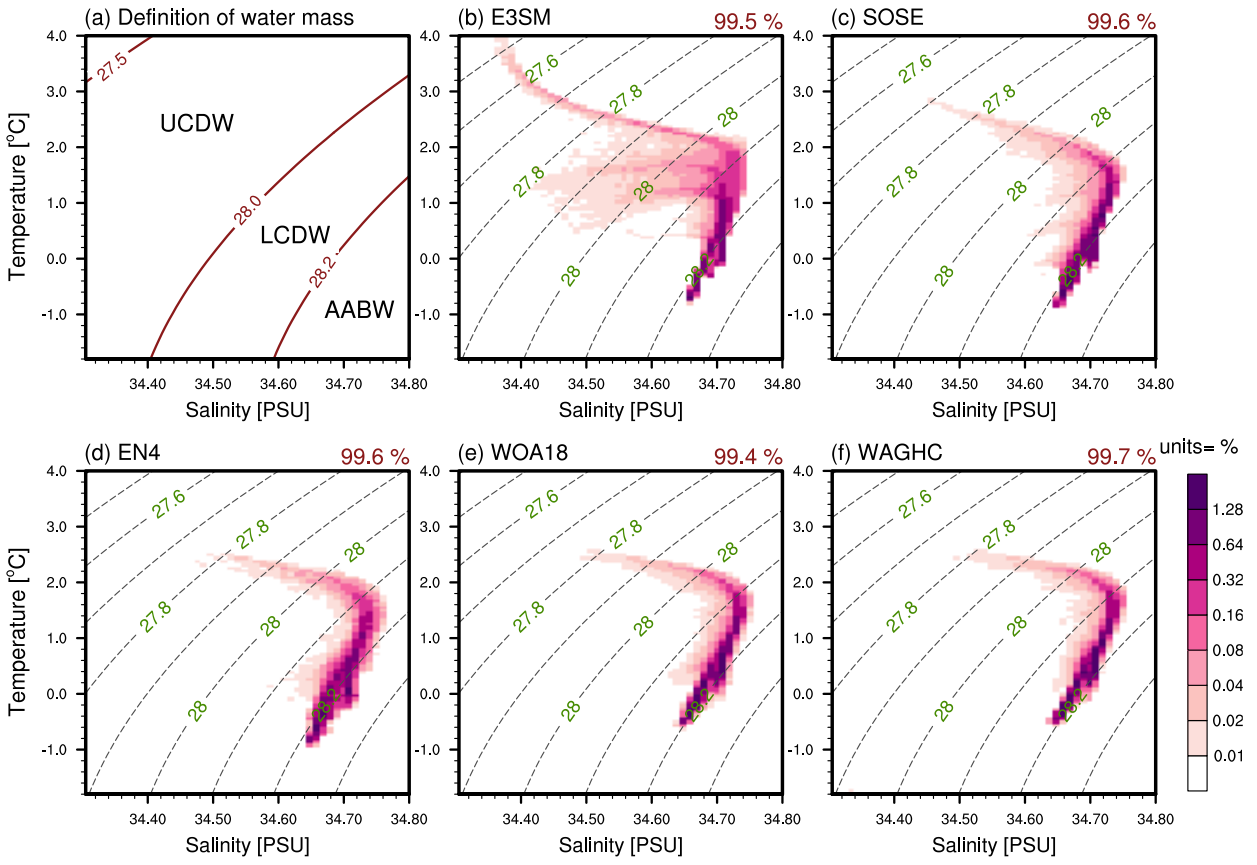

FIG. 3. (a) Definition of water masses in this study and volumetric probability density functions (PDFs) of Southern Ocean annual mean temperature and salinity for the region south of 60°S and over the entire depth range from (b) E3SM Ctrl, (c) SOSE, (d) EN4, (e) WOA18, and (f) WAGHC. The units are the percentage of the total volume of the region with the given properties. Summation of PDFs are displayed in the upper right corner of each figure (with difference relative to 100% indicating the percentage of values falling outside of the T and S ranges plotted here). Dashed contour lines denote neutral density, γ_n. We also define Surface Water ($\gamma_n < 27.5\ \mathrm{kg\,m^{-3}}$), but that is located outside of this T-S diagram.

Accepted for publication in *Journal of Climate*. DOI 10.1175/JCLI-D-19-0683.1.

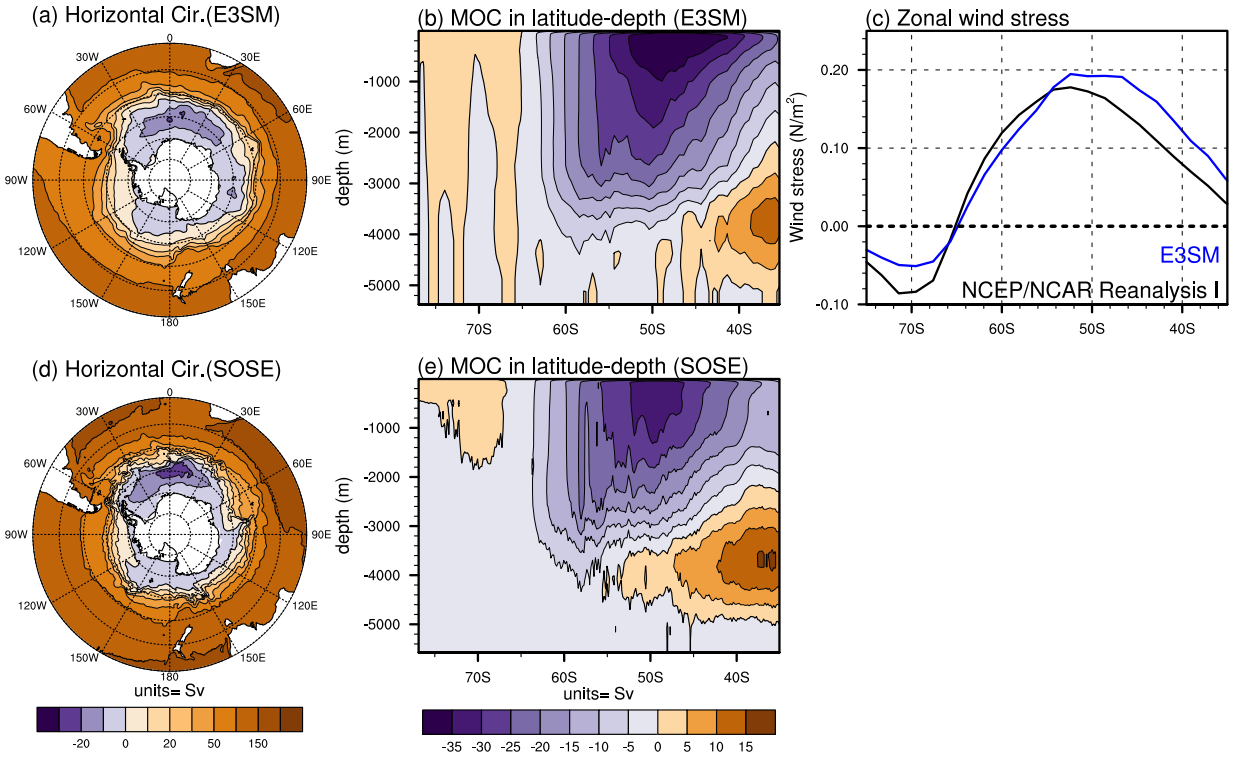

872 FIG. 4. Mean vertical integrated transport streamfunction (Sv) from (a) E3SM (Ctrl simulation) and (d) SOSE.
873 The zero contour is the Antarctic coast and the contour interval is 10 Sv. Positive values denote anticyclonic
874 subtropical gyres and negative values denote cyclonic polar gyres. Southern Ocean overturning streamfunction
875 (Sv) from (b) E3SM and (e) SOSE for latitude-depth spaces. The contour interval is 5 Sv. Positive values
876 represent counterclockwise and negative represent clockwise circulations. (c) Zonally averaged zonal wind
877 stress for E3SM and NCEP/NCAR Reanalysis I. Positive values of wind stress means westerly winds (West to
878 East) and negative values are easterly winds (East to West).

Accepted for publication in *Journal of Climate*. DOI 10.1175/JCLI-D-19-0683.1.

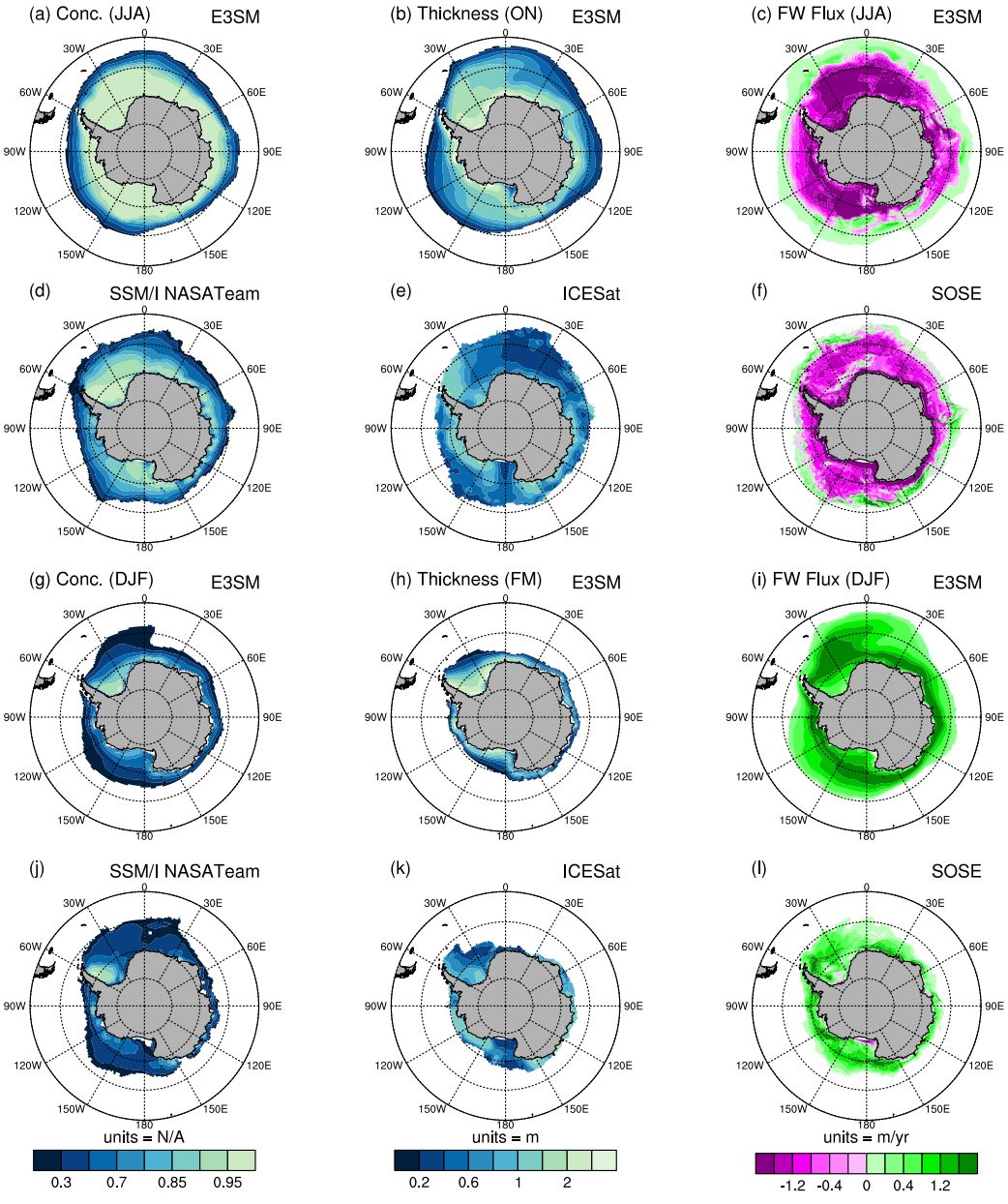

FIG. 5. June-July-August mean sea-ice concentration (a and d), October-November mean sea-ice thickness (b and e), and June-July-August mean freshwater flux from sea-ice into ocean (c and f) from E3SM (30-year mean from the Ctrl simulation), SSM/I NASATeam, ICESat, and SOSE (6-year mean). December-January-February mean sea-ice concentration (g and j), February-March mean sea-ice thickness (h and k), and December-January-February mean freshwater flux from sea-ice into ocean (i and l) from E3SM (30-year mean from the Ctrl simulation), SSM/I NASATeam, ICESat, and SOSE (6-year mean). The figures only display sea-ice with concentration greater than 0.15 (15%) and thickness greater than 10cm.

Accepted for publication in *Journal of Climate*. DOI 10.1175/JCLI-D-19-0683.1.

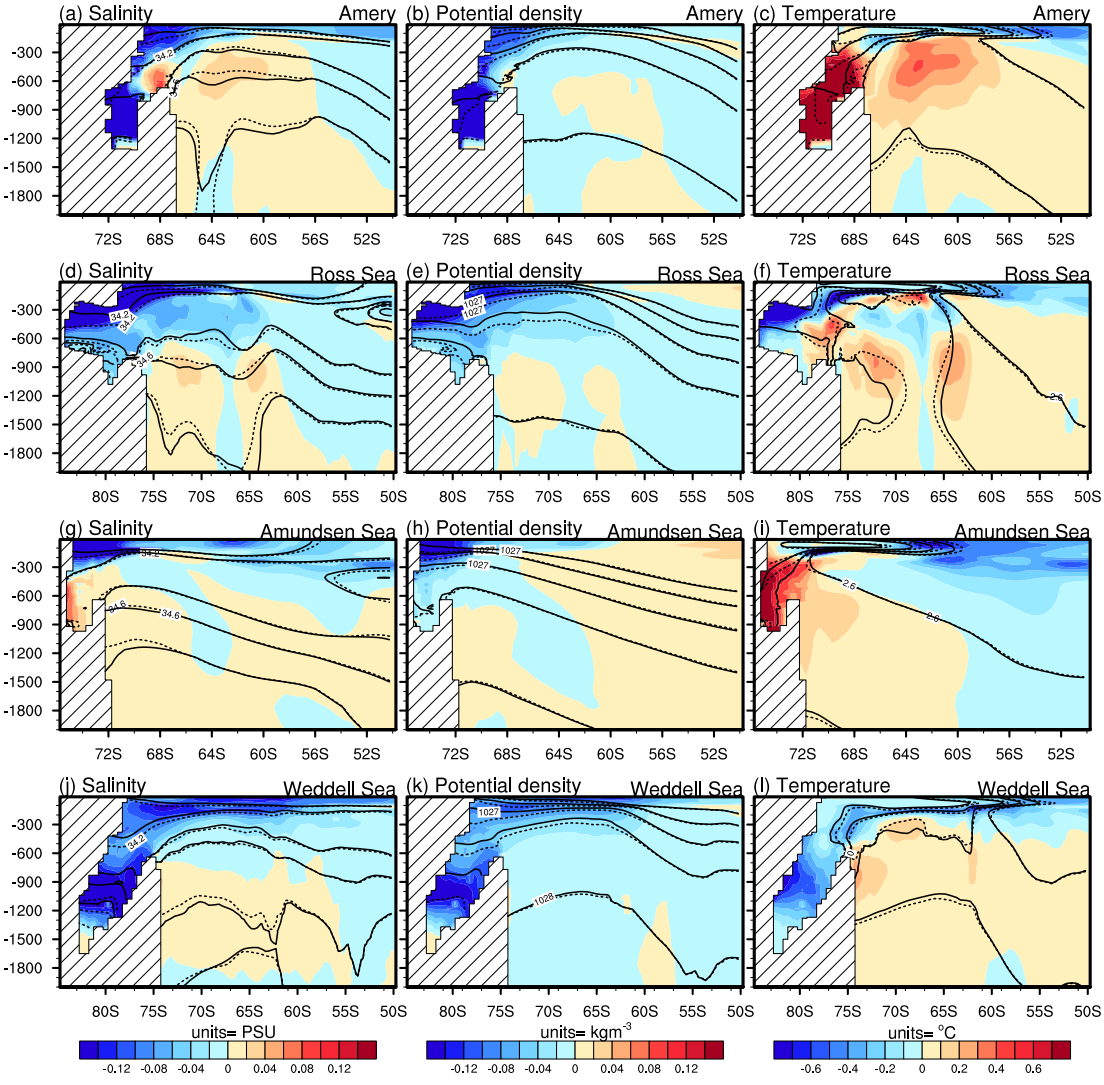

886 FIG. 6. Vertical cross sections of differences in zonally averaged (left) salinity, (middle) potential density,
887 and (right) ocean temperature between the ISM and Ctrl simulations (ISM - Ctrl) for the Amery Ice-shelf sector
888 [60°E-90°E], Ross Sea [165°E-165°W], Amundsen Sea [90°W-120°W], and Weddell Sea [60°W-30°W]. Solid
889 lines are isohaline, isopycnals, and isotherms for the Ctrl simulation and dashed lines are for the ISM simulation.

Accepted for publication in *Journal of Climate*. DOI 10.1175/JCLI-D-19-0683.1.

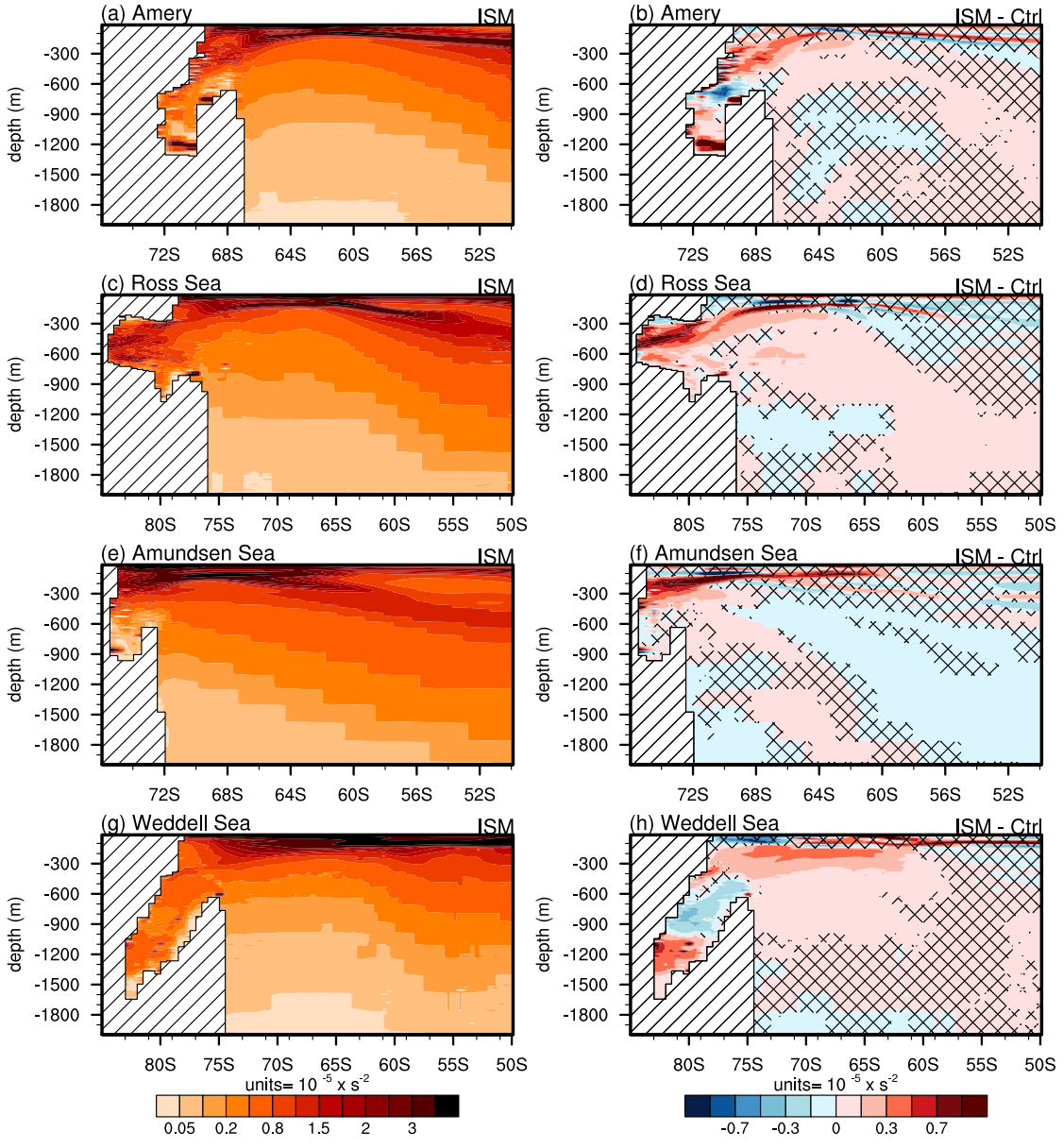

FIG. 7. Vertical density stratification ($N^2 = -(g/\rho_0)d\rho/dz$) in the (a) Amery ice-shelf sector [60°E-90°E], (c) Ross Sea [165°E-165°W], (e) Amundsen Sea [90°W-120°W], (g) Weddell sea [60°W-30°W] from the ISM simulations (left) and differences between the ISM and Ctrl simulations (ISM - Ctrl) (right). The stippled area represents non-significant differences at the 95% confidence level from Student's t-test.

Accepted for publication in *Journal of Climate*. DOI 10.1175/JCLI-D-19-0683.1.

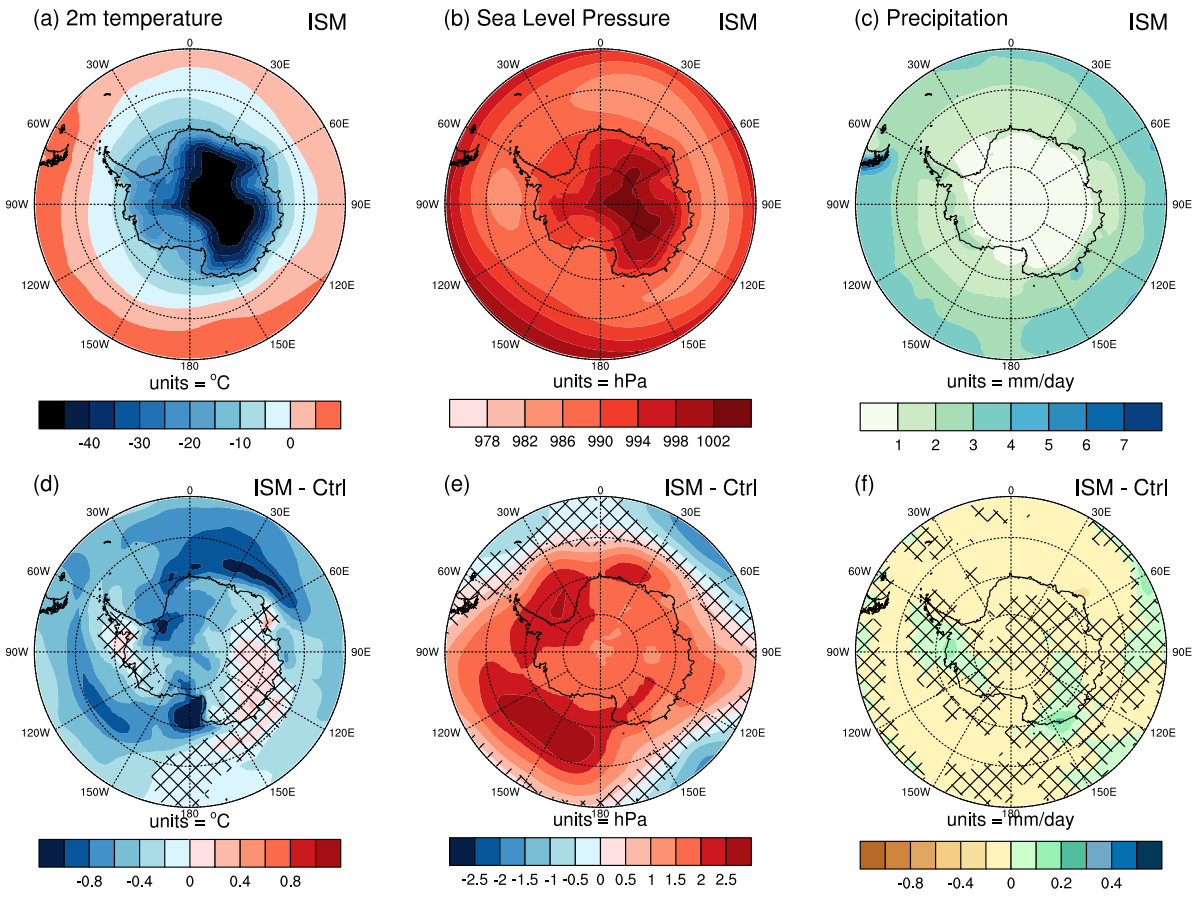

894 FIG. 8. Annual mean (a) 2m temperature, (b) sea level pressure and (c) precipitation from the ISM simulation
895 and differences between the ISM and Ctrl simulations (ISM - Ctrl) in (d) 2m temperature, (e) sea level pressure
896 and (f) precipitation. The stippled area represents non-significant differences at the 95% confidence level from
897 Student's t-test.

Accepted for publication in *Journal of Climate*. DOI 10.1175/JCLI-D-19-0683.1.

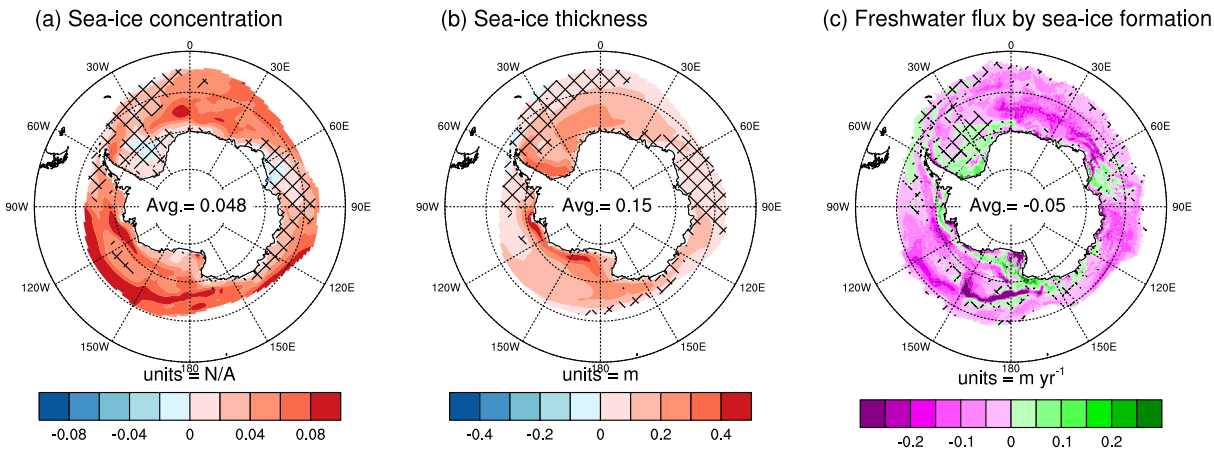

FIG. 9. Differences between the ISM and Ctrl simulations (ISM - Ctrl) in annual mean sea-ice concentration (a), sea-ice thickness (b), and freshwater flux from sea-ice freezing (c). For freshwater flux by sea-ice formation (c), negative values represent more sea-ice freezing and positive values mean less sea-ice freezing. Area averaged values for each field are displayed in the middle of each plot. The stippled area represents non-significant differences at the 95% confidence level from Student's t-test.

Accepted for publication in *Journal of Climate*. DOI 10.1175/JCLI-D-19-0683.1.

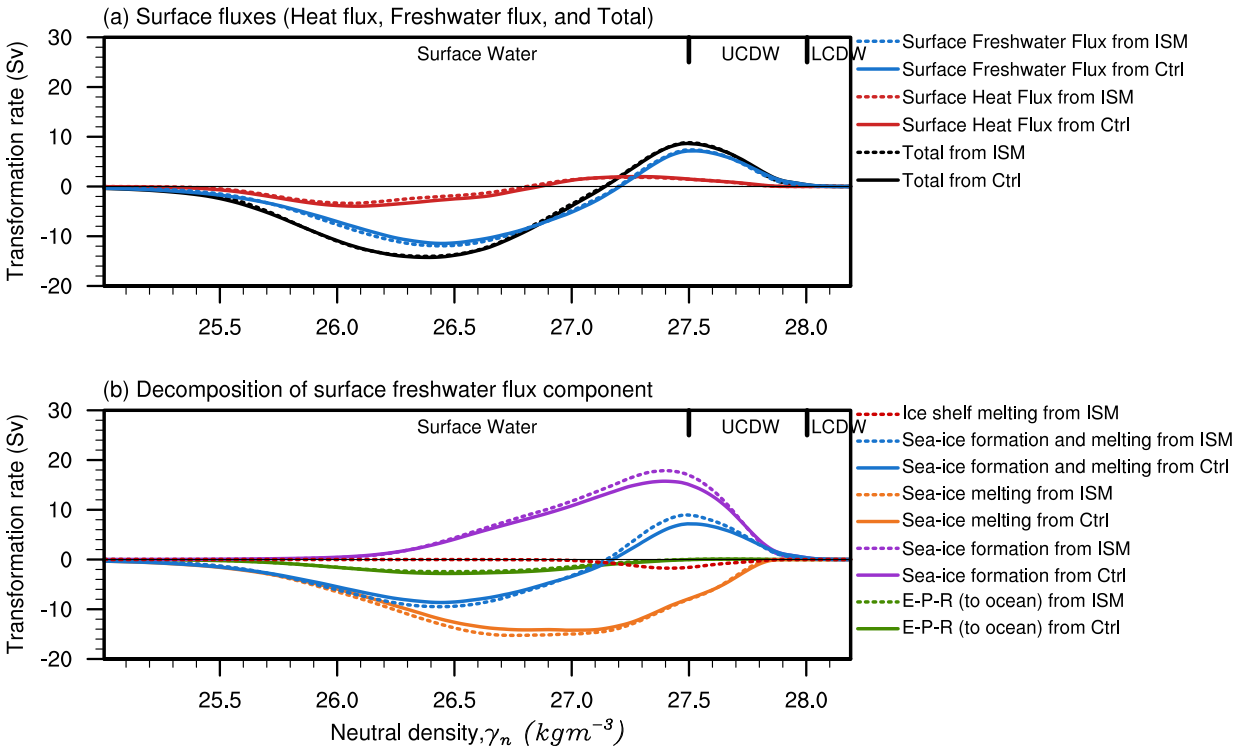

FIG. 10. WMT rates due to individual surface-flux types from the ISM simulation (dashed lines) and the Ctrl simulation (solid lines) over the Southern Ocean south of 60°S. (a) The decomposition of transformation from surface heat flux and freshwater flux into the Southern Ocean, and their sum. (b) The decomposition of transformation rate from surface freshwater flux into E-P-R (Evaporation, Precipitation, and Runoff), sea-ice formation and melting, and ice-shelf melting. Note the runoff term (R) has a solid ice and liquid water component, with both distributed to coastal grid cells.

Accepted for publication in *Journal of Climate*. DOI 10.1175/JCLI-D-19-0683.1.

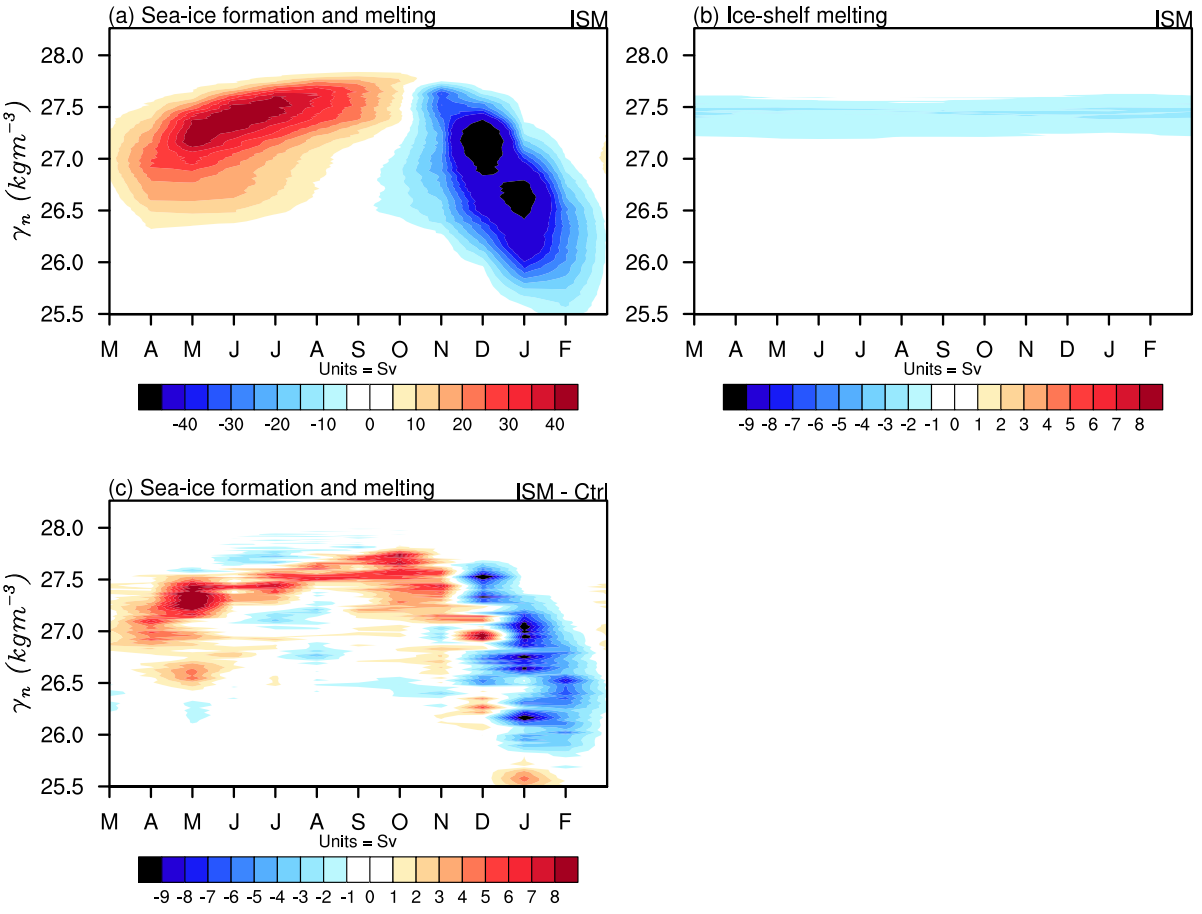

909 FIG. 11. Climatological annual cycle of WMT rate caused by freshwater flux from sea-ice formation and
910 melting (a) and from ice-shelf melting (b) for the ISM. (c) Differences of WMT rate caused by freshwater flux
911 from sea-ice formation and melting between two simulations, as a function of time (x-axis) and neutral density,
912 γ_n (y-axis).

Accepted for publication in *Journal of Climate*. DOI 10.1175/JCLI-D-19-0683.1.

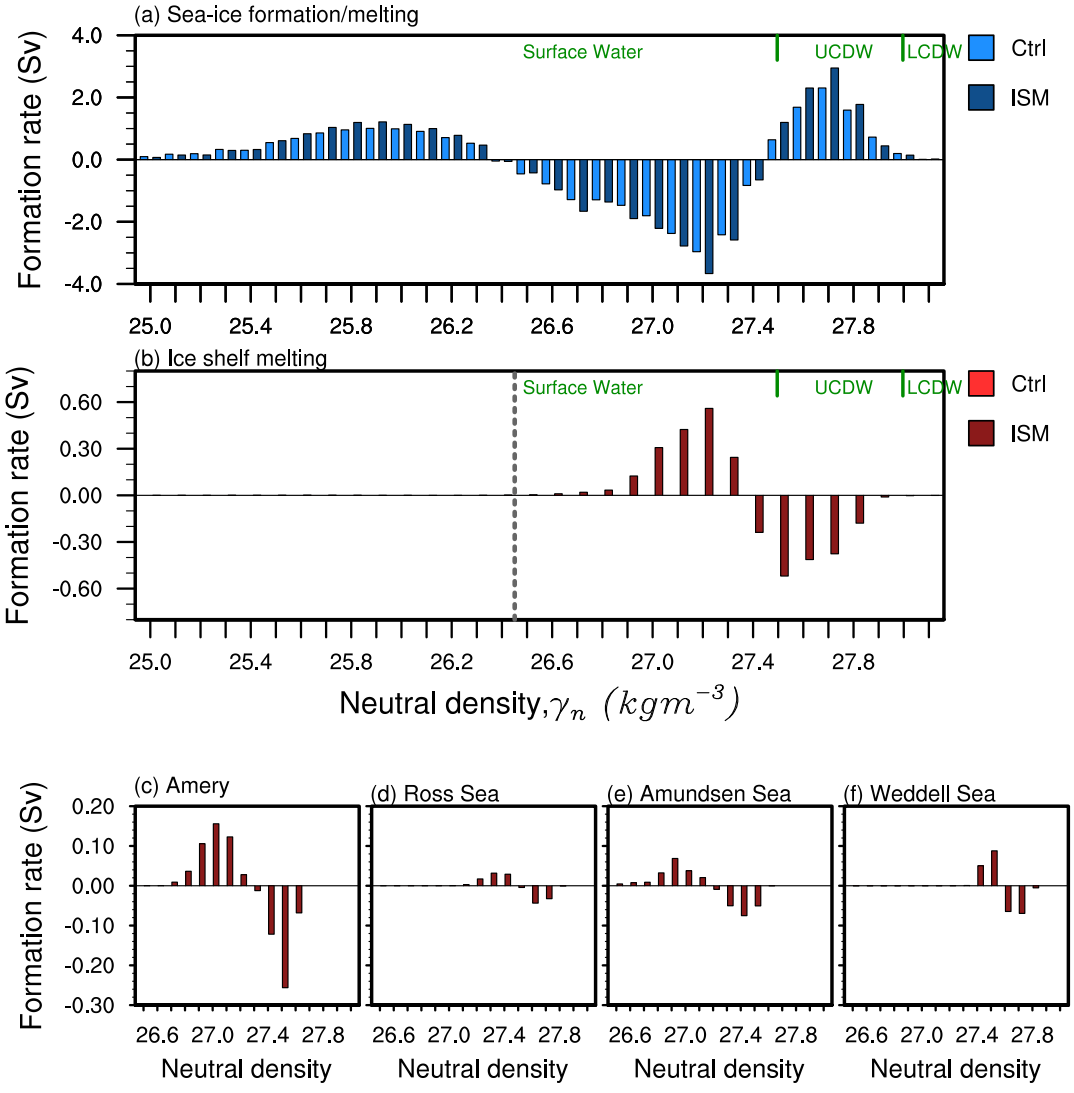

913 FIG. 12. Water mass formation rates in the Ctrl and ISM simulations by freshwater flux component (a and
914 b), summed in 0.1 kg m^{-3} neutral density bins. Water mass formation rate by freshwater flux from (a) sea-ice
915 formation and melting and (b) ice-shelf melting. Regional water mass formation rate by ice-shelf melting over
916 the (c) Amery ice-shelf sector [60°E-90°E], (d) Ross Sea [165°E-165°W], (e) Amundsen Sea [90°W-120°W],
917 and (f) Weddell Sea [60°W-30°W]. Regional water mass formation rates are only plotted above 26.5 kg m^{-3}
918 neutral density level, shown as the dotted line in (b).

Accepted for publication in *Journal of Climate*. DOI 10.1175/JCLI-D-19-0683.1.